EUROPEAN ORGANIZATION FOR NUCLEAR RESEARCH (CERN)

CERN-PH-EP/2012-240
2013/01/29

CMS-SUS-12-003

Search for supersymmetry in events with b-quark jets and missing transverse energy in pp collisions at 7 TeV

The CMS Collaboration*

Abstract

Results are presented from a search for physics beyond the standard model based on events with large missing transverse energy, at least three jets, and at least one, two, or three b-quark jets. The study is performed using a sample of proton-proton collision data collected at $\sqrt{s} = 7$ TeV with the CMS detector at the LHC in 2011. The integrated luminosity of the sample is 4.98 fb^{-1}. The observed number of events is found to be consistent with the standard model expectation, which is evaluated using control samples in the data. The results are used to constrain cross sections for the production of supersymmetric particles decaying to b-quark-enriched final states in the context of simplified model spectra.

Submitted to Physical Review D

*See Appendix A for the list of collaboration members

1 Introduction

Many extensions of the standard model (SM) predict that events in high-energy proton-proton collisions can contain large missing transverse energy ($E_{\mathrm{T}}^{\mathrm{miss}}$) and multiple, high-transverse momentum (p_{T}) jets. For example, in R-parity-conserving [1] models of supersymmetry (SUSY) [2], SUSY particles are created in pairs. Each member of the pair initiates a decay chain that terminates with the lightest SUSY particle (LSP) and SM particles. If the LSP only interacts weakly, as in the case of a dark-matter candidate, it escapes detection, potentially yielding significant $E_{\mathrm{T}}^{\mathrm{miss}}$. Furthermore, in some scenarios [3], the SUSY partners of the bottom and top quarks can be relatively light, leading to the enhanced production of events with bottom-quark jets (b jets). Events of this type, with b jets and large $E_{\mathrm{T}}^{\mathrm{miss}}$, represent a distinctive topological signature that is the subject of a search described in this paper.

We present a search for new physics (NP) in events with large $E_{\mathrm{T}}^{\mathrm{miss}}$, no isolated leptons, three or more high-p_{T} jets, and at least one, two, or three b jets. The analysis is based on a sample of proton-proton collision data collected at $\sqrt{s} = 7\,\mathrm{TeV}$ with the Compact Muon Solenoid (CMS) detector at the CERN Large Hadron Collider (LHC) in 2011, corresponding to an integrated luminosity of $4.98\,\mathrm{fb}^{-1}$. Recent searches for NP in a similar final state are presented in Refs. [4–8]. Our analysis is characterized by a strong reliance on techniques that use control samples in data to evaluate the SM background.

The principal sources of the SM background are events with top quarks, comprising $\mathrm{t\bar{t}}$ pair and single-top-quark events, events with a W or Z boson accompanied by jets, and non-top multijet events produced purely through strong-interaction processes. We hereafter refer to this last class of events as "QCD" background. Diboson (WW, ZZ, or WZ) events represent a smaller source of background. For events with a W boson or a top quark, significant $E_{\mathrm{T}}^{\mathrm{miss}}$ can arise if a W boson decays into a charged lepton and a neutrino. The neutrino provides a source of genuine $E_{\mathrm{T}}^{\mathrm{miss}}$. Similarly, significant $E_{\mathrm{T}}^{\mathrm{miss}}$ can arise in events with a Z boson if the Z boson decays to two neutrinos. For QCD background events, significant $E_{\mathrm{T}}^{\mathrm{miss}}$ arises primarily from the mismeasurement of jet p_{T}. A smaller component of the QCD background arises from events with semileptonic decays of b and c quarks.

We interpret our results in the context of simplified model spectra (SMS) [9–12], which provide a general framework to characterize NP signatures. They include only a few NP particles and focus on generic topologies. We consider the SMS scenarios denoted T1bbbb and T1tttt. Event diagrams are shown in Fig. 1. These two models are characterized by b-jet-enriched final states, large jet multiplicities, and large $E_{\mathrm{T}}^{\mathrm{miss}}$ values, making our analysis sensitive to their production. For convenience, we express SMS phenomenology using SUSY nomenclature. In T1bbbb (T1tttt), pair-produced gluinos $\tilde{\mathrm{g}}$ each decay into two b-quark jets (t-quark jets) and the LSP, taken to be the lightest neutralino $\tilde{\chi}^0$. The LSP is assumed to escape detection, leading to significant $E_{\mathrm{T}}^{\mathrm{miss}}$. If the SUSY partner of the bottom quark (top quark) is much lighter than any other squark, with the gluino yet lighter, gluino decays are expected to be dominated by the three-body process shown in Fig. 1(a) [Fig. 1(b)].

As benchmark NP scenarios, we choose the T1bbbb and T1tttt models with gluino mass $m_{\tilde{\mathrm{g}}} = 925\,\mathrm{GeV}$ and LSP mass $m_{\mathrm{LSP}} = 100\,\mathrm{GeV}$, with normalization to the next-to-leading order (NLO) plus next-to-leading-logarithm (NLL) cross section [13–17]. These two benchmark models lie near the boundary of our expected sensitivity.

In Sections 2-3 we describe the detector and event selection. Section 4 introduces the $\Delta\hat{\phi}_{\mathrm{min}}$ variable, used in the evaluation of the QCD background. Our techniques to evaluate the SM background from control samples in data are presented in Section 5. In Section 6 we describe

our analysis framework, based on a likelihood method that simultaneously determines the SM background and tests the consistency of NP models with the data, taking into account possible NP contamination of control sample regions. The interpretation of our results is presented in Section 7. A summary of the analysis is given in Section 8.

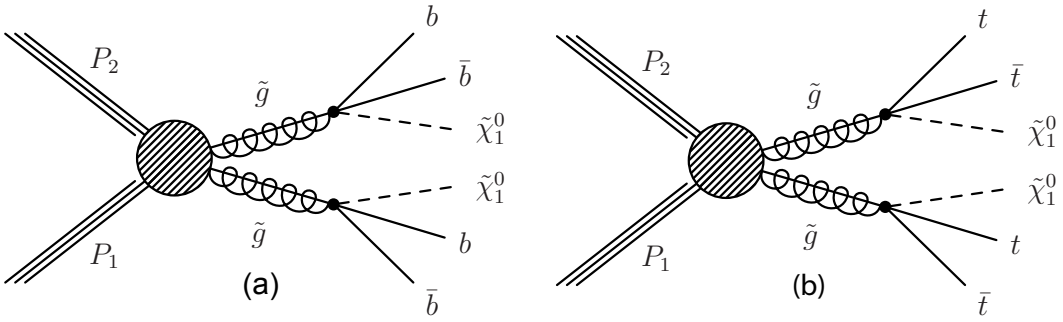

Figure 1: Event diagrams for the (a) T1bbbb and (b) T1tttt simplified models.

2 Detector and trigger

A detailed description of the CMS detector is given elsewhere [18]. The CMS coordinate system is defined with the origin at the center of the detector and the z axis along the direction of the counterclockwise beam. The transverse plane is perpendicular to the beam axis, with ϕ the azimuthal angle (measured in radians), θ the polar angle, and $\eta = -\ln[\tan(\theta/2)]$ the pseudorapidity. A superconducting solenoid provides an axial magnetic field of 3.8 T. Within the field volume are a silicon pixel and strip tracker, a crystal electromagnetic calorimeter, and a brass-scintillator hadron calorimeter. Muons are detected with gas-ionization chambers embedded in the steel flux-return yoke outside the solenoid. The tracker covers the region $|\eta| < 2.5$ and the calorimeters $|\eta| < 3.0$. The region $3 < |\eta| < 5$ is instrumented with a forward calorimeter. The near-hermeticity of the detector permits accurate measurements of energy balance in the transverse plane.

The principal trigger used for the analysis selects events based on the quantities H_T and H_T^{miss}, where H_T is the scalar sum of the transverse energy of jets and H_T^{miss} the modulus of the corresponding vector sum. Due to increasing beam collision rates, trigger conditions varied over the period of data collection. The most stringent trigger requirements were $H_T > 350$ GeV and $H_T^{miss} > 110$ GeV. The efficiency of the H_T component for the final event selection is measured from data to be 86% (99%) for H_T values of 400 GeV (500 GeV). The efficiency of the H_T^{miss} component is 98% for $E_T^{miss} > 250$ GeV. Appropriate corrections are applied to account for trigger inefficiencies and uncertainties in the various control and search regions of the analysis.

3 Event selection

Physics objects are defined using the particle flow (PF) method [19], which is used to reconstruct and identify charged and neutral hadrons, electrons (with associated bremsstrahlung photons), muons, tau leptons, and photons, using an optimized combination of information from CMS subdetectors. The PF objects serve as input for jet reconstruction, based on the anti-k_T algorithm [20] with distance parameter 0.5. Jet corrections [21] are applied to account for residual effects of non-uniform detector response in both p_T and η. The missing transverse energy E_T^{miss} is defined as the modulus of the vector sum of the transverse momenta of all PF objects. The E_T^{miss} vector is the negative of the same vector sum.

Table 1: The definition of the signal (SIG) regions. The minimum requirements on H_{T}, $E_{\mathrm{T}}^{\mathrm{miss}}$, and the number of tagged b jets $N_{\mathrm{b}jets}$ are given. The designations 1b, 2b, and 3b refer to the minimum $N_{\mathrm{b}jets}$ value, while "loose" and "tight" refer to less restrictive and more restrictive selection requirements, respectively, for H_{T} and $E_{\mathrm{T}}^{\mathrm{miss}}$.

Signal region		H_{T} [GeV]	$E_{\mathrm{T}}^{\mathrm{miss}}$ [GeV]	N_{bjets}
1b-loose	1BL	> 400	> 250	≥ 1
1b-tight	1BT	> 500	> 500	≥ 1
2b-loose	2BL	> 400	> 250	≥ 2
2b-tight	2BT	> 600	> 300	≥ 2
3b	3B	> 400	> 250	≥ 3

The basic event selection criteria are as follows:

- at least one well-defined primary event vertex [22];
- at least three jets with $p_{\mathrm{T}} > 50\,\mathrm{GeV}$ and $|\eta| < 2.4$;
- a lepton veto defined by requiring that there be no identified, isolated electron or muon candidate [23, 24] with $p_{\mathrm{T}} > 10\,\mathrm{GeV}$; electron candidates are restricted to $|\eta| < 2.5$ and muon candidates to $|\eta| < 2.4$;
- $\Delta\hat{\phi}_{\mathrm{min}} > 4.0$, where the $\Delta\hat{\phi}_{\mathrm{min}}$ variable is described in Section 4.

Electrons and muons are considered isolated if the scalar sum of the transverse momenta of charged hadrons, photons, and neutral hadrons surrounding the lepton within a cone of radius $\sqrt{(\Delta\eta)^2 + (\Delta\phi)^2} = 0.3$, divided by the lepton p_{T} value itself, is less than 0.20 for electrons and 0.15 for muons.

To identify b jets, we use the combined-secondary-vertex algorithm at the medium working point [25]. This algorithm combines information about secondary vertices, track impact parameters, and jet kinematics, to separate b jets from light-flavored-quark, charm-quark, and gluon jets. To increase sensitivity to NP scenarios, which often predict soft b jets, we use all tagged b jets with $p_{\mathrm{T}} > 30\,\mathrm{GeV}$. The nominal b-jet-tagging efficiency is about 75% for jets with a p_{T} value of 100 GeV, as determined from a sample of b-jet-enriched dijet events [25] (for b jets with $p_{\mathrm{T}} \approx 30\,\mathrm{GeV}$, this efficiency is about 60%). The corresponding misidentification rate is about 1.0%. We correct the simulated efficiencies for b-jet tagging and misidentification to match the efficiencies measured with control samples in the data. The b-tagging correction factor depends slightly on the jet p_{T} and has a typical value of 0.95. The uncertainty on this correction factor varies from 0.03 to 0.07 for b jets with p_{T} from 30 to 670 GeV, and is taken to be 0.13 for b jets with $p_{\mathrm{T}} > 670\,\mathrm{GeV}$.

We define five signal regions, which partially overlap, to enhance sensitivity in different kinematic regimes. The five regions correspond to different minimum requirements on H_{T}, $E_{\mathrm{T}}^{\mathrm{miss}}$, and the number of b jets. H_{T} is calculated using jets with $p_{\mathrm{T}} > 50\,\mathrm{GeV}$ and $|\eta| < 2.4$. The five regions, denoted 1BL, 1BT, 2BL, 2BT, and 3B, are specified in Table 1 and were chosen without considering the data to avoid possible bias. The regions are selected based on expected signal and background event yields in simulation, to provide maximal sensitivity for discovery of the NP scenarios considered in this paper or, in the case of non-discovery, to best set limits on their parameters. Throughout this paper, we use the generic designation "SIG" to refer to any or all of these five signal regions.

The distributions of the number of tagged b jets for the 1BL, 1BT, and 2BT samples (i.e., for the three different sets of selection criteria on H_{T} and $E_{\mathrm{T}}^{\mathrm{miss}}$), except without the requirement on the number of b jets, are shown in Fig. 2. The results are presented in comparison with

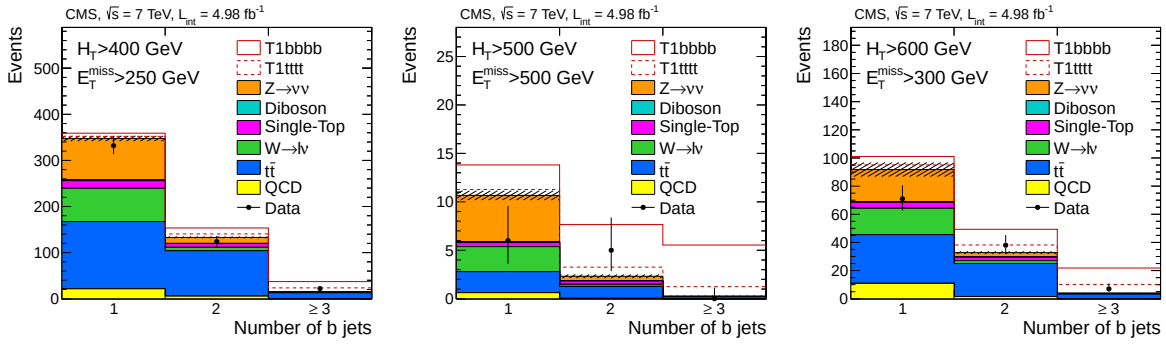

Figure 2: The distributions of the number of tagged b jets for event samples selected with the (a) 1BL, (b) 1BT, and (c) 2BT requirements, except for the requirement on the number of b jets. The hatched bands show the statistical uncertainty on the total SM background prediction from simulation. The open histograms show the expectations for the T1bbbb (solid line) and T1tttt (dashed line) NP models, both with $m_{\tilde{g}} = 925\,\text{GeV}$, $m_{\text{LSP}} = 100\,\text{GeV}$, and normalization to NLO+NLL.

Monte Carlo (MC) simulations of SM processes. Results from the benchmark T1bbbb and T1tttt NP models mentioned in the Introduction are also shown. The simulated $\text{t}\bar{\text{t}}$, W+jets, and Z+jets events are produced at the parton level with the MADGRAPH5.1.1.0 [26] event generator. Single-top-quark events are generated with the POWHEG 301 [27] program. The PYTHIA 6.4.22 program [28] is used to produce diboson and QCD events. For all simulated samples, PYTHIA 6.4 is used to describe parton showering and hadronization. All samples are generated using the CTEQ6 [29] parton distribution functions. The description of the detector response is implemented using the GEANT4 [30] program. The $\text{t}\bar{\text{t}}$ sample is normalized to the measured cross section [31]. The other simulated samples are normalized using the most accurate cross section calculations currently available, which is generally NLO. The jet energy resolution in the simulation is corrected to account for a small discrepancy with respect to data [21]. In addition, the simulated samples are reweighted to describe the probability distribution observed in data for overlapping pp collisions within a bunch crossing ("pileup").

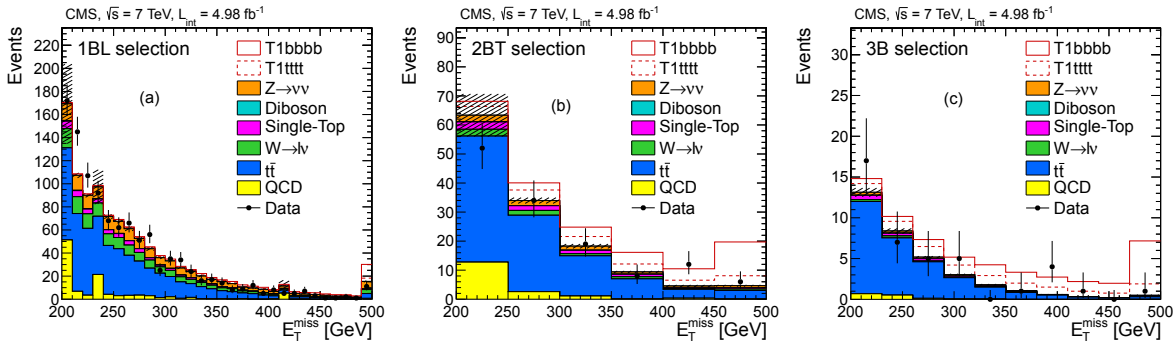

Figure 3: The distributions of $E_{\text{T}}^{\text{miss}}$ for event samples selected with the (a) 1BL, (b) 2BT, and (c) 3B requirements, except for the requirement on $E_{\text{T}}^{\text{miss}}$. The simulated spectra are normalized as in Fig. 2. The hatched bands show the statistical uncertainty on the total SM background prediction from simulation. The rightmost bin in all plots includes event overflow. The open histograms show the expectations for the T1bbbb (solid line) and T1tttt (dashed line) NP models, both with $m_{\tilde{g}} = 925\,\text{GeV}$, $m_{\text{LSP}} = 100\,\text{GeV}$, and normalization to NLO+NLL.

As examples illustrating the characteristics of events with at least one, two, or three tagged b

Table 2: The number of data events and corresponding predictions from MC simulation for the signal regions, with normalization to 4.98 fb^{-1}. The uncertainties on the simulated results are statistical.

	1BL	1BT	2BL	2BT	3B
Data	478	11	146	45	22
Total SM MC	496 ± 7	13.3 ± 0.6	148 ± 2	36.8 ± 0.9	15.0 ± 0.2
$t\bar{t}$	257 ± 2	3.6 ± 0.2	111 ± 1	26.7 ± 0.4	12.6 ± 0.2
Single-top quark	26.0 ± 1.0	0.8 ± 0.2	9.1 ± 0.5	2.7 ± 0.3	0.88 ± 0.09
W+jets	80.0 ± 1.0	2.8 ± 0.2	7.7 ± 0.3	2.2 ± 0.2	0.38 ± 0.05
$Z \to \nu\bar{\nu}$	104 ± 2	5.3 ± 0.4	13.8 ± 0.7	3.5 ± 0.3	0.80 ± 0.10
Diboson	1.8 ± 0.1	0.10 ± 0.02	0.27 ± 0.04	0.05 ± 0.02	0.02 ± 0.01
QCD	28.0 ± 6.0	0.70 ± 0.20	6.0 ± 1.0	1.7 ± 0.6	0.29 ± 0.07

jets, the $E_{\mathrm{T}}^{\mathrm{miss}}$ distributions of events in the 1BL, 2BT, and 3B samples are shown in Fig. 3. The numbers of events in the different signal regions are listed in Table 2 for data and simulation. The simulated results are for guidance only and are not used in the analysis.

4 The $\Delta\hat{\phi}_{\mathrm{min}}$ variable

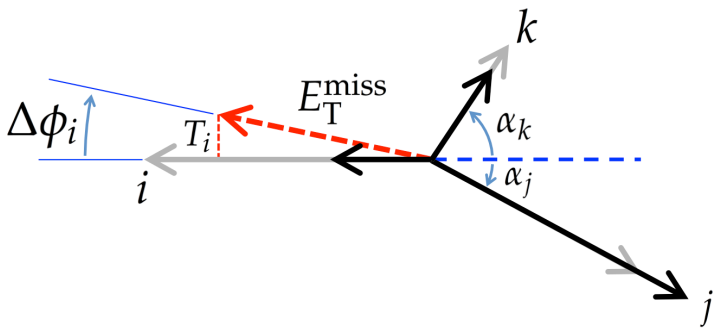

Figure 4: Illustration of variables used to calculate $\Delta\hat{\phi}_{\mathrm{min}}$ for the case of an event with exactly three jets with $p_{\mathrm{T}} > 30$ GeV. The light-shaded (light gray) solid arrows show the true p_{T} values of the three jets i, j, and k. The dark-shaded (black) solid arrows show the reconstructed jet p_{T} values. The angles of jets j and k with respect to the direction opposite to jet i are denoted α_j and α_k. The $E_{\mathrm{T}}^{\mathrm{miss}}$ for the event is shown by the dotted (red) arrow. The component of $E_{\mathrm{T}}^{\mathrm{miss}}$ perpendicular to jet i, denoted T_i, is shown by the dotted (red) line. σ_{T_i} is the uncertainty on T_i. $\Delta\phi_i$ is the angle between $E_{\mathrm{T}}^{\mathrm{miss}}$ and jet i.

Our method to evaluate the QCD background is based on the $\Delta\hat{\phi}_{\mathrm{min}}$ variable. This method presumes that most $E_{\mathrm{T}}^{\mathrm{miss}}$ in a QCD event arises from the p_{T} mismeasurement of a single jet.

The $\Delta\hat{\phi}_{\mathrm{min}}$ variable is a modified version of the commonly used quantity $\Delta\phi_{\mathrm{min}} \equiv \min(\Delta\phi_i)$ ($i = 1, 2, 3$), the minimum azimuthal opening angle between the $E_{\mathrm{T}}^{\mathrm{miss}}$ vector and each of the three highest-p_{T} jets in an event. Misreconstruction of a jet primarily affects the modulus of its transverse momentum but not its direction. Thus QCD background events are characterized by small values of $\Delta\phi_{\mathrm{min}}$. The $\Delta\phi_{\mathrm{min}}$ variable is strongly correlated with $E_{\mathrm{T}}^{\mathrm{miss}}$, as discussed below. This correlation undermines its utility for the evaluation of the QCD background from data. To reduce this correlation, we divide the $\Delta\phi_i$ by their estimated resolutions $\sigma_{\Delta\phi,i}$ to obtain $\Delta\hat{\phi}_{\mathrm{min}} \equiv \min(\Delta\phi_i/\sigma_{\Delta\phi,i})$.

The resolution $\sigma_{\Delta\phi,i}$ for jet i is evaluated by considering the $p_{\rm T}$ resolution $\sigma_{p_{\rm T}}$ of the other jets in the event. The uncertainty σ_{T_i} on the component of the $E_{\rm T}^{\rm miss}$ vector perpendicular to jet i is found using $\sigma_{T_i}^2 \equiv \sum_n (\sigma_{p_{{\rm T},n}} \sin\alpha_n)^2$, where the sum is over all other jets in the event with $p_{\rm T} > 30$ GeV and α_n is the angle between jet n and the direction opposite jet i. The situation is depicted in Fig. 4 for an event with exactly three jets with $p_{\rm T} > 30$ GeV. Our estimate of the $\Delta\phi$ resolution is $\sigma_{\Delta\phi,i} = \arctan(\sigma_{T_i}/E_{\rm T}^{\rm miss})$. [Note: $\arcsin(\sigma_{T_i}/E_{\rm T}^{\rm miss})$ is technically more correct in this expression; we use $\arctan(\sigma_{T_i}/E_{\rm T}^{\rm miss})$ because it is computationally more robust while being equivalent for the small angles of interest here.] For the jet $p_{\rm T}$ resolution, it suffices to use the simple linear parametrization $\sigma_{p_{\rm T}} = 0.10\, p_{\rm T}$ [21].

Figure 5(a) shows the ratio of the number of events with $\Delta\phi_{\rm min} > 0.3$ to the number with $\Delta\phi_{\rm min} < 0.3$ as a function of $E_{\rm T}^{\rm miss}$, for a simulated QCD sample selected with the 1BL requirements except for those on $\Delta\hat{\phi}_{\rm min}$ and $E_{\rm T}^{\rm miss}$ ($\Delta\phi_{\rm min} > 0.3$ or a similar criterion is commonly used to reject QCD background, see, e.g., Refs. [5–8]). The strong correlation between $\Delta\phi_{\rm min}$ and $E_{\rm T}^{\rm miss}$ is evident. The corresponding result based on $\Delta\hat{\phi}_{\rm min}$ is shown in Fig. 5(b). For the latter figure we choose $\Delta\hat{\phi}_{\rm min} = 4.0$ in place of $\Delta\phi_{\rm min} = 0.3$, which yields a similar selection efficiency. For values of $E_{\rm T}^{\rm miss}$ greater than about 30 GeV, the distribution based on $\Delta\hat{\phi}_{\rm min}$ is seen to be far less dependent on $E_{\rm T}^{\rm miss}$ than that based on $\Delta\phi_{\rm min}$. Figure 5(c) shows the result corresponding to Fig. 5(b) for events with zero tagged b jets. Comparing Figs. 5(b) and (c), it is seen that the ratio $N(\Delta\hat{\phi}_{\rm min} \geq 4.0)/N(\Delta\hat{\phi}_{\rm min} < 4.0)$ has an approximately constant value of about 0.13 (for $E_{\rm T}^{\rm miss} > 30$ GeV) irrespective of the number of b jets.

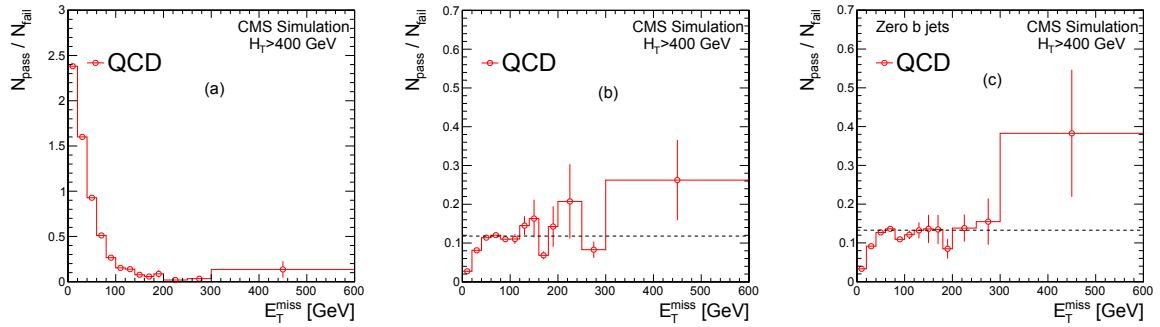

Figure 5: QCD-simulation results: (a) the ratio of the number of events that pass the criterion $\Delta\phi_{\rm min} \geq 0.3$ ($N_{\rm pass}$) to the number that fail ($N_{\rm fail}$) as a function of $E_{\rm T}^{\rm miss}$, for events selected with the 1BL requirements except for those on $\Delta\hat{\phi}_{\rm min}$ and $E_{\rm T}^{\rm miss}$; (b) The analogous ratio of events with $\Delta\hat{\phi}_{\rm min} \geq 4.0$ to those with $\Delta\hat{\phi}_{\rm min} < 4.0$; and (c) the same as (b) for events with zero b jets. The QCD-background estimate is based on the relative flatness of the distributions in (b) and (c) for $E_{\rm T}^{\rm miss} \gtrsim 30$ GeV, as illustrated schematically by the dashed lines.

The measured results for $N(\Delta\hat{\phi}_{\rm min} \geq 4.0)/N(\Delta\hat{\phi}_{\rm min} < 4.0)$ with zero b jets, for events with $H_{\rm T} > 400$ GeV, 500 GeV, and 600 GeV, are shown in Fig. 6. By requiring that there not be a b jet, we reduce the contribution of top-quark events, which is helpful for the evaluation of QCD background (Section 5.1). The data in Fig. 6 are collected with a pre-scaled $H_{\rm T}$ trigger, allowing events to be selected at low $E_{\rm T}^{\rm miss}$ without a trigger bias. The data in Fig. 6(a) are seen to somewhat exceed the simulated predictions. The trend is visible in Fig. 6(b) to a lesser extent. This modest discrepancy arises because the $\Delta\hat{\phi}_{\rm min}$ distribution is narrower in the simulation than in data. Since our method to evaluate the QCD background is based on the measured distribution, this feature of the simulation does not affect our analysis. The data in Fig. 6 are seen to exhibit the general behavior expected from the simulation. The region below around 100 GeV is seen to be dominated by the QCD background.

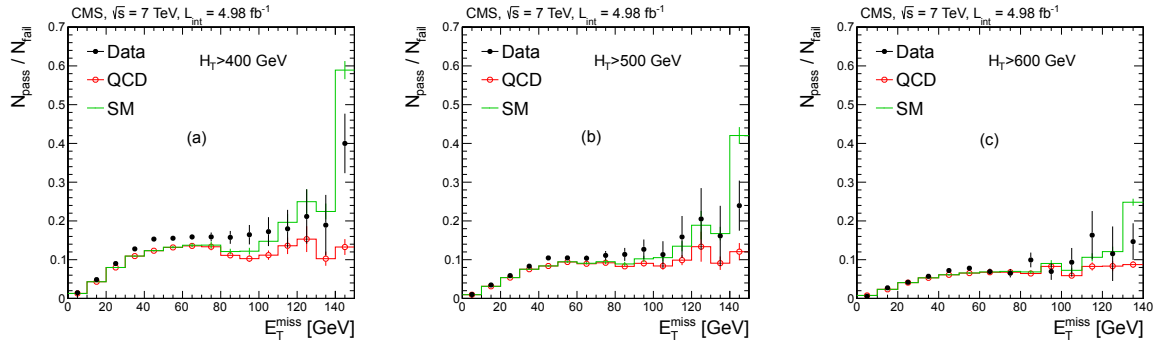

Figure 6: The ratio $N(\Delta\hat{\phi}_{\min} \geq 4.0)/N(\Delta\hat{\phi}_{\min} < 4.0)$, denoted N_{pass}/N_{fail}, as a function of E_T^{miss} for the zero-b-jet sample, for events selected with the basic event selection criteria of the analysis except for the requirements on E_T^{miss} and the number of b jets. The results are shown for (a) $H_T > 400$ GeV, (b) $H_T > 500$ GeV, and (c) $H_T > 600$ GeV. The histograms show simulated predictions for the QCD and total SM background.

5 Background evaluation

In this section we describe our methods to evaluate the SM background from control samples in data. Each of the three main backgrounds – from QCD, Z+jets, and top-quark and W+jets events (where "top quark" includes both $t\bar{t}$ and single-top-quark events) – is evaluated separately. We group top quark and W+jets events together because they have a similar experimental signature. Note that our final results for the total SM background are derived from a global likelihood procedure that incorporates our background evaluation procedures into a single fit, and that also accounts for possible NP contributions to the control regions in a consistent manner. The global likelihood procedure is described in Section 6.

QCD background is evaluated using the $\Delta\hat{\phi}_{\min}$ variable. Background from Z+jets events is evaluated by scaling the measured rates of $Z \to \ell^+\ell^-$ (ℓ = e or μ) events. To estimate the top-quark and W+jet background, we employ two complementary techniques. One, which we call the nominal method, is simple and almost entirely data based, while the other, which we call the E_T^{miss}-reweighting method, combines results based on data with information from simulation to examine individual sources of top-quark and W+jets background in detail.

5.1 QCD background

The low level of correlation between $\Delta\hat{\phi}_{\min}$ and E_T^{miss} allows us to employ a simple method to evaluate the QCD background from data. As discussed in Section 4, the ratio $N(\Delta\hat{\phi}_{\min} \geq 4.0)/N(\Delta\hat{\phi}_{\min} < 4.0)$ is approximately independent of E_T^{miss}, and also of the number of b jets, for QCD events. Furthermore, the E_T^{miss} distribution below 100 GeV is expected to be dominated by QCD events, especially for events with zero b jets (Fig. 6). We therefore measure $N(\Delta\hat{\phi}_{\min} \geq 4.0)/N(\Delta\hat{\phi}_{\min} < 4.0)$ in a low E_T^{miss} region of the zero-b-jet sample and assume this equals $N(\Delta\hat{\phi}_{\min} \geq 4.0)/\ N(\Delta\hat{\phi}_{\min} < 4.0)$ for QCD events at all E_T^{miss} values, also for samples with b jets such as our signal samples.

To perform this measurement, we divide the data into sideband and signal regions in the $\Delta\hat{\phi}_{\min}$-E_T^{miss} plane, as illustrated schematically in Fig. 7. We use the low-E_T^{miss} interval defined by $50 < E_T^{miss} < 100$ GeV and $\Delta\hat{\phi}_{\min} > 4.0$. We call this interval the low sideband (LSB) region. We also define low $\Delta\hat{\phi}_{\min}$ (LDP) intervals $\Delta\hat{\phi}_{\min} < 4.0$. We do this not only for the $50 < E_T^{miss} < 100$ GeV region, but also for the signal regions (SIG) and for a sideband (SB) region defined by $150 < E_T^{miss} < 250$ GeV. We denote these regions LSB-LDP, SIG-LDP, and SB-LDP, respectively. The LSB-LDP region is dominated by QCD events. Similarly, the SB-LDP and SIG-LDP regions

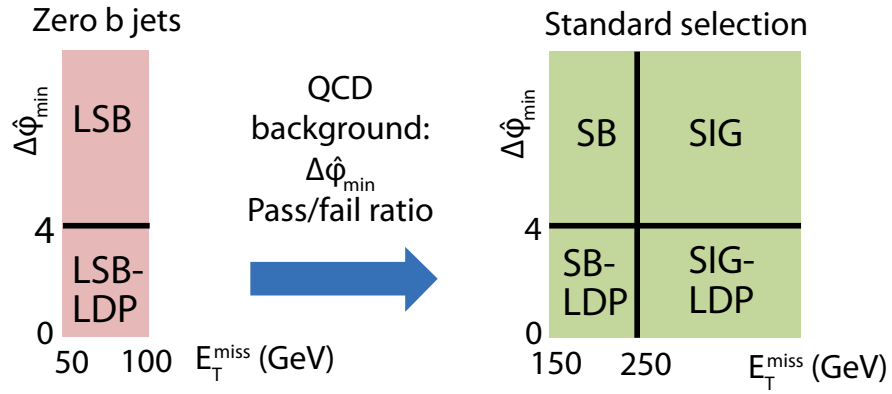

Figure 7: Schematic diagram illustrating the regions used to evaluate the QCD background. The low sideband (LSB) and low sideband-low $\Delta\hat{\phi}_{\text{min}}$ (LSB-LDP) regions correspond to $50 < E_{\text{T}}^{\text{miss}} < 100\,\text{GeV}$. The sideband (SB) and sideband-low $\Delta\hat{\phi}_{\text{min}}$ (SB-LDP) regions correspond to $150 < E_{\text{T}}^{\text{miss}} < 250\,\text{GeV}$. The signal (SIG) and signal-low $\Delta\hat{\phi}_{\text{min}}$ (SIG-LDP) regions have $E_{\text{T}}^{\text{miss}}$ ranges corresponding to those in Table 1. The designation "SIG" generically refers to any of the signal regions in this table. The SIG and SIG-LDP regions shown in the diagram explicitly depict the loose kinematic signal regions 1BL, 2BL, and 3B, which require $E_{\text{T}}^{\text{miss}} > 250\,\text{GeV}$, but implicitly include the tight kinematic signal regions 1BT and 2BT, which require $E_{\text{T}}^{\text{miss}} > 500\,\text{GeV}$ and $300\,\text{GeV}$, respectively. For each choice of signal region, the condition on H_{T} specified in Table 1 for that region is applied to all six panels of the diagram, while the condition on the number of b jets is applied to the four panels denoted "Standard selection." All regions with the low $\Delta\hat{\phi}_{\text{min}}$ (LDP) designation require $0.0 < \Delta\hat{\phi}_{\text{min}} < 4.0$, while the other regions require $\Delta\hat{\phi}_{\text{min}} > 4.0$.

Table 3: The relative systematic uncertainties (%) for the QCD background estimate in the signal regions. Because the 1BT QCD background estimate is zero (Section 5.5), we do not present results for 1BT in this table.

	1BL	2BL	2BT	3B
MC subtraction	23	43	44	24
MC closure	37	41	150	45
LSB reweighting	7.9	7.9	9.8	7.9
Total	44	60	160	52

largely consist of QCD events, as illustrated for the 1BL, 2BT, and 3B SIG-LDP regions in Fig. 8 (according to simulation, QCD events comprise between 73% and 85% of the events in the SB-LDP region, depending on the SIG selection; the corresponding results for for the SIG-LDP region lie between 50% and 70%). For higher values of $E_{\mathrm{T}}^{\mathrm{miss}}$, contributions to the SB-LDP and SIG-LDP regions from events with a top quark or a W or Z boson become more important. This contamination is subtracted using simulation.

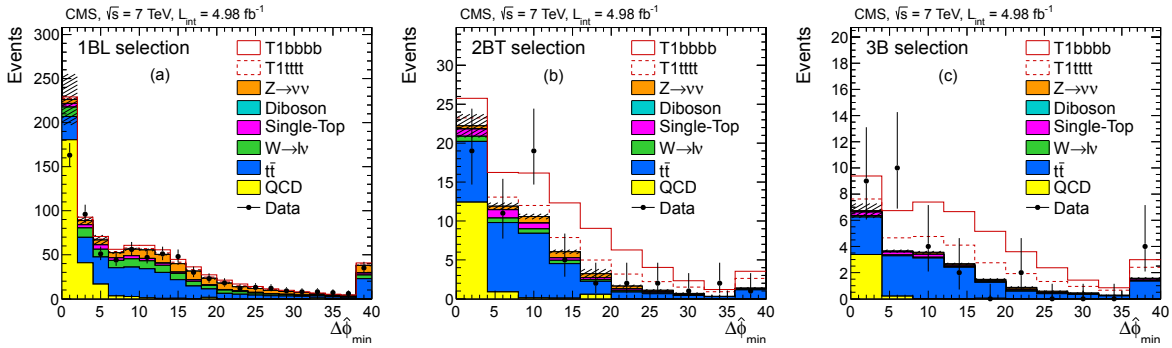

Figure 8: The distributions of $\Delta\hat{\phi}_{\mathrm{min}}$ in data and simulation for events selected with the (a) 1BL, (b) 2BT, and (c) 3B requirements, except for the requirement on $\Delta\hat{\phi}_{\mathrm{min}}$. The simulated spectra are normalized as in Fig. 2. The hatched bands show the statistical uncertainty on the total SM prediction from simulation. The open histograms show the expectations for the T1bbbb (solid line) and T1tttt (dashed line) NP models, both with $m_{\tilde{\mathrm{g}}} = 925\,\mathrm{GeV}$, $m_{\mathrm{LSP}} = 100\,\mathrm{GeV}$, and normalization to NLO+NLL. The SIG-LDP regions correspond to $\Delta\hat{\phi}_{\mathrm{min}} < 4.0$ and the signal (SIG) regions to $\Delta\hat{\phi}_{\mathrm{min}} > 4.0$.

Applying corrections for the non-QCD components of the SIG-LDP and SB-LDP regions, our estimates of the QCD yields in the SIG and SB regions are therefore:

$$N_{\mathrm{SIG}}^{\mathrm{QCD}} = \frac{N_{\mathrm{LSB}}}{N_{\mathrm{LSB-LDP}}} \times (N_{\mathrm{SIG-LDP}} - N_{\mathrm{SIG-LDP}}^{\mathrm{top,MC}} - N_{\mathrm{SIG-LDP}}^{\mathrm{W\&Z,MC}}), \quad (1)$$

$$N_{\mathrm{SB}}^{\mathrm{QCD}} = \frac{N_{\mathrm{LSB}}}{N_{\mathrm{LSB-LDP}}} \times (N_{\mathrm{SB-LDP}} - N_{\mathrm{SB-LDP}}^{\mathrm{top,MC}} - N_{\mathrm{SB-LDP}}^{\mathrm{W\&Z,MC}}), \quad (2)$$

where the LSB and LSB-LDP results are derived from the zero-b-jet, pre-scaled H_{T} trigger sample mentioned in Section 4. The result for $N_{\mathrm{SB}}^{\mathrm{QCD}}$ is used in Section 5.3. The ratio $N_{\mathrm{LSB}}/N_{\mathrm{LSB-LDP}}$ is found to depend on the number of primary vertices (PV) in the event and thus on the LHC instantaneous luminosity. Before evaluating Eqs. (1) and (2), we therefore reweight the events in the pre-scaled sample to have the same PV distribution as the standard sample.

Systematic uncertainties are summarized in Table 3. The systematic uncertainty associated with the subtraction of events with either a top quark or a W or Z boson from the SIG-LDP and

SB-LDP regions is determined by varying the subtracted values by their uncertainties, evaluated as described in Section 7. The systematic uncertainty associated with the assumption that $E_{\mathrm{T}}^{\mathrm{miss}}$ and $\Delta\hat{\phi}_{\mathrm{min}}$ are uncorrelated is evaluated with an MC closure test, namely by determining the ability of the method to predict the correct yield using simulated samples. We compute $(N_{\mathrm{true}} - N_{\mathrm{pred}})/N_{\mathrm{pred}}$, where N_{pred} is the predicted number of QCD events in the signal region, estimated by applying the above procedure to simulated samples treated as data, and N_{true} is the true number. We assign the result, added in quadrature with its statistical uncertainty, as a symmetric systematic uncertainty. This uncertainty is dominated by statistical uncertainties for N_{true}. The closure test is performed both for the standard simulated samples and for simulated samples that are reweighted to account for discrepancies in the jet multiplicity distributions between data and simulation; we take the larger closure discrepancy as the uncertainty. A third systematic uncertainty is evaluated by taking $\pm 100\%$ of the shift in the result caused by the PV reweighting of $N_{\mathrm{LSB}}/N_{\mathrm{LSB-LDP}}$. The systematic uncertainty associated with the trigger efficiency is found to be negligible.

As a cross-check, we vary the definition of the LSB by raising and lowering its lower edge by 10 GeV, which alters the number of events in the LSB by more than a factor of two in each case. The observed change in the QCD background estimate is negligible.

5.2 Z+jets background

Events with a Z boson and one or more b jets present an irreducible background when the Z decays to two neutrinos. We evaluate this background by reconstructing $\mathrm{Z} \to \ell^+\ell^-$ events ($\ell =$ e or μ) and removing the ℓ^+ and ℓ^-. Fits are performed to determine the $\mathrm{Z} \to \ell^+\ell^-$ yields, which are then corrected for background and efficiency. The efficiency is $\epsilon = \mathcal{A} \cdot \epsilon_{\mathrm{trig}} \cdot \epsilon^2_{\ell\,\mathrm{reco}} \cdot \epsilon^2_{\ell\,\mathrm{sel}}$, where the geometrical acceptance $\mathcal{A}$ is determined from simulation while the trigger ϵ_{trig}, lepton reconstruction $\epsilon_{\ell\,\mathrm{reco}}$, and lepton selection $\epsilon_{\ell\,\mathrm{sel}}$ efficiencies are determined from data. The corrected $\mathrm{Z} \to \ell^+\ell^-$ yields are used to estimate the $\mathrm{Z} \to \nu\overline{\nu}$ background through scaling by the ratio of branching fractions, $\mathrm{BR}(\mathrm{Z} \to \nu\overline{\nu})/\mathrm{BR}(\mathrm{Z} \to \ell^+\ell^-) = 5.95 \pm 0.02$ [32], after accounting for the larger acceptance of $\mathrm{Z} \to \nu\overline{\nu}$ events.

The $\mathrm{Z} \to \ell^+\ell^-$ yields are small or zero in the signal regions. To increase these yields, we select events with the signal-sample requirements except with a significantly looser b-tagging definition. A scale factor derived from a control sample in data is then applied to estimate the number of $\mathrm{Z} \to \ell^+\ell^-$ events in the signal regions. The control sample is defined with the same loosened b-tagging definition, but without requiring the presence of a Z boson, and also by reversing the $\Delta\hat{\phi}_{\mathrm{min}}$ requirement, i.e., we require $\Delta\hat{\phi}_{\mathrm{min}} < 4.0$, which yields a control sample with a b-jet content similar to that in the $\mathrm{Z} \to \ell^+\ell^-$ and $\mathrm{Z} \to \nu\overline{\nu}$ events. All other selection criteria are the same as for the corresponding signal sample. The scale factors are given by the fraction of events in the control sample that passes the nominal b-tagging requirements. The scale factors have values around 0.30, 0.07, and 0.01 for the samples with ≥ 1, ≥ 2, and ≥ 3 b jets, respectively. We verify that the output of the b-tagging algorithm is independent of the presence of a Z.

We validate our method with a consistency test, applying the above procedure to data samples with loosened restrictions on H_{T} and $E_{\mathrm{T}}^{\mathrm{miss}}$. We find the number of predicted and observed $\mathrm{Z} \to \ell^+\ell^-$ events to be in close agreement.

Systematic uncertainties are summarized in Table 4. We evaluate a systematic uncertainty on the scale factors by loosening and tightening the b-tagging criterion of the control sample and taking half the difference between the two results as an uncertainty. The size of the control sample changes by about $\pm 30\%$ in these variations. In addition, we use $\Delta\hat{\phi}_{\mathrm{min}} > 4.0$ rather

Table 4: The relative systematic uncertainties (%) for the $Z \to \nu\bar{\nu}$ background estimate in the signal regions, determined for $Z \to e^+e^-$ ($Z \to \mu^+\mu^-$) events.

	1BL	1BT	2BL	2BT	3B
Scale factors	17 (20)	17 (20)	49 (61)	49 (61)	140 (110)
Non-resonant $\ell^+\ell^-$ background	10 (8)	10 (8)	10 (8)	10 (8)	10 (8)
Acceptance	3 (3)	6 (8)	3 (3)	4 (4)	3 (3)
Lepton selection efficiency	5 (4)	5 (4)	5 (4)	5 (4)	5 (4)
Trigger efficiency	5 (5)	5 (5)	5 (5)	5 (5)	5 (5)
MC closure	11 (19)	11 (19)	11 (19)	11 (19)	11 (19)
Total	24 (30)	25 (30)	52 (65)	52 (65)	150 (110)

than $\Delta\hat{\phi}_{\text{min}} < 4.0$ to define the control sample and calculate the difference with respect to the nominal results. Finally, we evaluate the percentage difference between the number of predicted and observed events found with the consistency test described above. The three terms are added in quadrature to define the systematic uncertainty of the scale factors. We evaluate a systematic uncertainty associated with the non-resonant $\ell^+\ell^-$ background to $Z \to \ell^+\ell^-$ events by comparing the fraction of fitted events in the $Z \to \ell^+\ell^-$ peak from the nominal fit with those found using either a loosened H_T or a loosened E_T^{miss} restriction. The RMS of the three results is added in quadrature with the statistical uncertainty from the nominal fit to define the systematic uncertainty. The 1BL selection is used to determine this uncertainty for all signal regions. A systematic uncertainty for the acceptance is defined by recalculating the acceptance after varying the p_T and η ranges of the ℓ^+ and ℓ^-. The largest difference with respect to the nominal result is added in quadrature with the statistical uncertainty of the acceptance. A systematic uncertainty is defined for the lepton selection efficiency, and analogously for the trigger efficiency, by recalculating the respective efficiency after varying the requirements on H_T, E_T^{miss}, $\Delta\hat{\phi}_{\text{min}}$, the number of jets, and the number of b jets (the number of jets is found using all jets with $p_T > 50\,\text{GeV}$ and $|\eta| < 2.4$). We also use alternative signal and background shapes in the fits used to extract the $Z \to \ell^+\ell^-$ event yields. The maximum variations from each case are added in quadrature with the statistical uncertainty from the nominal method to define the systematic uncertainties. Finally, we evaluate a systematic uncertainty based on an MC closure test in the manner described in Section 5.1. We use the SB region to determine this uncertainty.

An analogous procedure to that described above is used to evaluate the number of $Z \to \nu\bar{\nu}$ events $N_{\text{SB}}^{Z\to\nu\bar{\nu}}$ in the SB regions ($150 < E_T^{\text{miss}} < 250\,\text{GeV}$), along with the corresponding uncertainty.

5.3 Top-quark and W+jets background (nominal)

For most signal regions, $t\bar{t}$ events are expected to be the dominant background (Table 2). Backgrounds from single-top-quark and W+jets events are expected to be smaller but to have a similar signature. Almost all top-quark and W+jets background in our analysis arises either because a W boson decays leptonically to an e or a μ, with the e or μ unidentified, not isolated, or outside the acceptance of the analysis, or because a W boson decays to a hadronically decaying τ lepton. We find empirically, through studies with simulation, that the shape of the E_T^{miss} distribution is similar for all top-quark and W+jets background categories that enter the signal (Table 1) or sideband ($150 < E_T^{\text{miss}} < 250\,\text{GeV}$) regions, regardless of whether the W boson decays to e, μ, or τ, or whether a τ lepton decays hadronically or leptonically: the decay of the W boson in W+jets events generates an E_T^{miss} spectrum (from the neutrino) that is similar to the E_T^{miss} spectrum generated by the W boson produced directly in the decay of a top quark in top quark events. Additional, softer neutrinos in events with a τ lepton do not much alter

this spectrum. We also find that this shape is well-modeled by the $E_{\mathrm{T}}^{\mathrm{miss}}$ distribution of a single-lepton (SL) control sample formed by inverting the lepton veto, i.e., by requiring that exactly one e or one μ be present using the lepton identification criteria of Section 3, in a sample whose selection is otherwise the same as the corresponding signal sample, except to reduce the potential contribution of NP to the SL samples, we impose an additional restriction $M_{\mathrm{T}} < 100\,\mathrm{GeV}$ on the SL samples (only), where M_{T} is the transverse W-boson mass formed from the charged lepton and $E_{\mathrm{T}}^{\mathrm{miss}}$ momentum vectors. As an illustration, Fig. 9 shows a comparison based on simulation of the $E_{\mathrm{T}}^{\mathrm{miss}}$ distributions in the signal and SL samples, for events selected with the 1BL, 2BT, and 3B criteria.

The $E_{\mathrm{T}}^{\mathrm{miss}}$ distributions of events in the SL samples with the 1BL, 2BT, and 3B requirements are shown in Fig. 10. The distributions are seen to be overwhelmingly composed of $\mathrm{t\bar{t}}$ events (for example, according to simulation, top and W+jets events comprise over 98% of the events in the SB-SL samples for all SIG selections). The expected contributions of the benchmark T1bbbb NP scenario are found to be negligible, while those of the benchmark T1tttt scenario are seen to be small in Fig. 10 compared to Fig. 3.

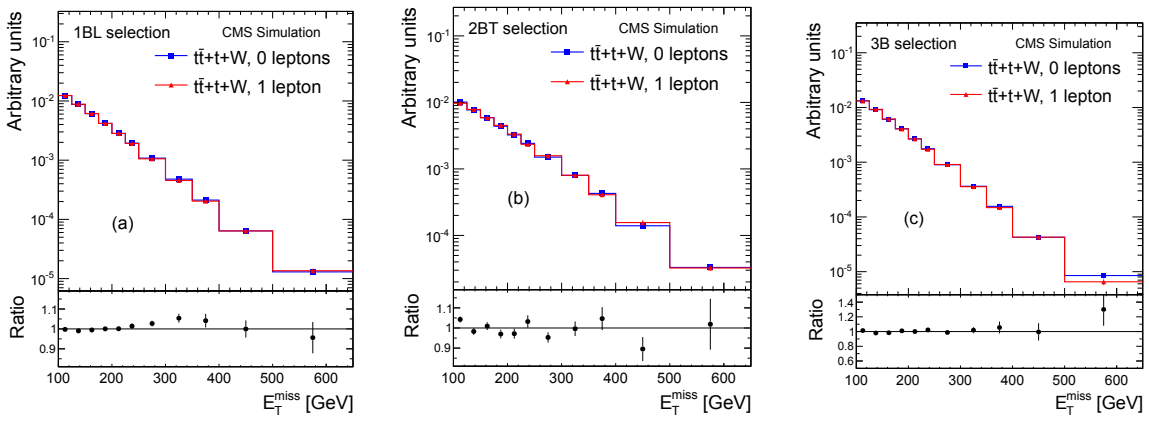

Figure 9: The distributions of $E_{\mathrm{T}}^{\mathrm{miss}}$ in simulated events selected with the (a) 1BL, (b) 2BT, and (c) 3B requirements, except for the requirement on $E_{\mathrm{T}}^{\mathrm{miss}}$. The square (triangle) symbols show the results for signal (single-lepton SL control) sample events. The small plots below the main figures show the ratio of the signal to SL sample curves. The event samples include $\mathrm{t\bar{t}}$, W+jet, and single-top-quark events.

Based on these observations, we implement a template method in which the shape of the $E_{\mathrm{T}}^{\mathrm{miss}}$ distribution in an SL sample is used to describe the shape of the $E_{\mathrm{T}}^{\mathrm{miss}}$ distribution in the corresponding signal sample of Table 1, for all top-quark and W+jets categories. An uncertainty for our presumption of the similarity of the $E_{\mathrm{T}}^{\mathrm{miss}}$ spectra between different top and W+jet categories is evaluated through the closure test described below. We split each SL sample into a sideband $E_{\mathrm{T}}^{\mathrm{miss}}$ region SB-SL defined by $150 < E_{\mathrm{T}}^{\mathrm{miss}} < 250\,\mathrm{GeV}$, and a signal $E_{\mathrm{T}}^{\mathrm{miss}}$ region SIG-SL given by the corresponding $E_{\mathrm{T}}^{\mathrm{miss}}$ requirement in Table 1. The templates are normalized based on the number of top-quark plus W+jets events observed in the SB regions ($150 < E_{\mathrm{T}}^{\mathrm{miss}} < 250\,\mathrm{GeV}$) of samples selected with the requirements of Table 1 except for that on $E_{\mathrm{T}}^{\mathrm{miss}}$. A schematic diagram of the different regions used to evaluate the top and W+jets background with the nominal method is presented in Fig. 11. Contributions to the SB region from QCD and $\mathrm{Z} \to \nu\bar{\nu}$ events are taken from the data-based estimates of Sections 5.1 and 5.2. Small, residual contributions from other backgrounds such as diboson events are subtracted using simulation.

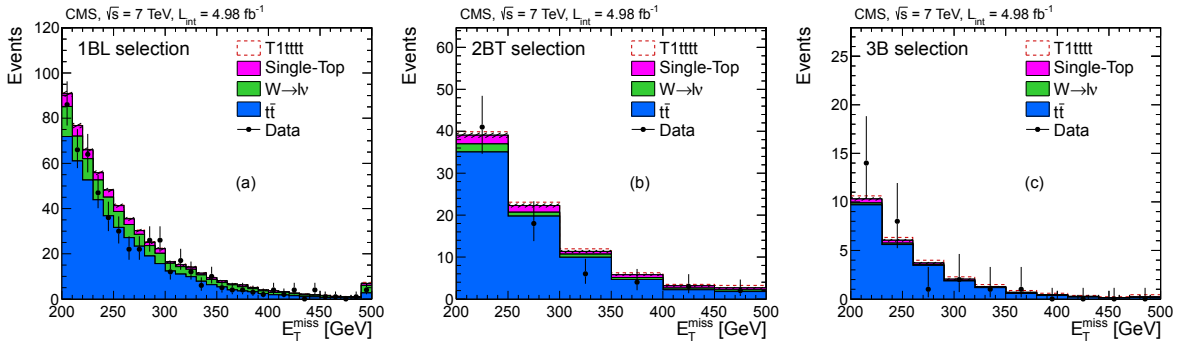

Figure 10: The distributions of $E_{\mathrm{T}}^{\mathrm{miss}}$ for the SL control sample for events selected with the (a) 1BL, (b) 2BT, and (c) 3B requirements, except for the requirement on $E_{\mathrm{T}}^{\mathrm{miss}}$. The simulated spectra are normalized as in Fig. 2. The hatched bands show the statistical uncertainty on the total SM prediction from simulation. The open dashed histogram shows the expectations for the T1tttt NP model with $m_{\tilde{\mathrm{g}}} = 925\,\mathrm{GeV}$, $m_{\mathrm{LSP}} = 100\,\mathrm{GeV}$, and normalization to NLO+NLL (the corresponding contributions from the T1bbbb model are negligible and are not shown).

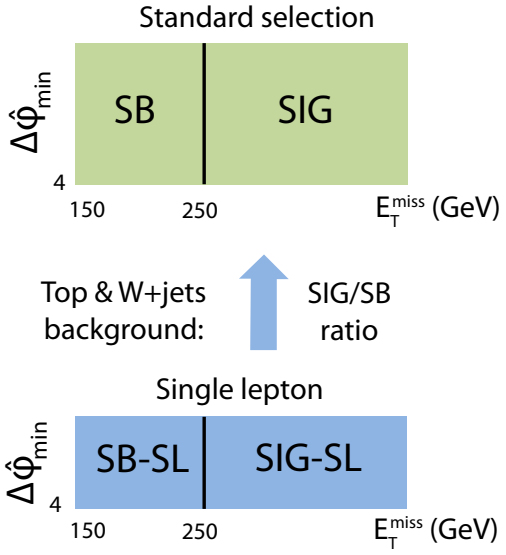

Figure 11: Schematic diagram illustrating the regions used to evaluate the top and W+jets background with the nominal method. The sideband (SB) and signal (SIG) regions are described in the caption to Fig. 7. The sideband-single-lepton (SB-SL) and signal-single-lepton (SIG-SL) regions correspond to the SB and SIG regions, respectively, except an electron or muon is required to be present and a requirement is placed on the transverse W boson mass $M_{\mathrm{T}} < 100\,\mathrm{GeV}$.

Table 5: The relative systematic uncertainties (%) for the nominal top-quark and W+jets background estimate in the signal regions.

	1BL	1BT	2BL	2BT	3B
MC closure	4.6	15	5.4	4.6	2.8
Subtraction of QCD	13	19	8.2	20	8.0
Subtraction of $Z \to \nu\bar{\nu}$	3.4	3.9	5.4	5.9	15
MC subtraction	0.6	0.6	0.2	0.4	0.1
Trigger efficiency	13	14	11	11	10
Total	19	28	15	24	20

Our estimate of the top-quark and W+jets background in the SIG region is therefore:

$$N_{\mathrm{SIG}}^{\mathrm{top+W}} = \frac{N_{\mathrm{SIG-SL}}}{N_{\mathrm{SB-SL}}} \times (N_{\mathrm{SB}} - N_{\mathrm{SB}}^{Z\to\nu\bar{\nu}} - N_{\mathrm{SB}}^{\mathrm{QCD}} - N_{\mathrm{SB}}^{\mathrm{other,MC}}). \quad (3)$$

Contamination of the SB region in the benchmark T1bbbb (T1tttt) NP scenario is predicted to be around 1% (1%) for the 1BL, 1BT, and 2BL selections, 4% (3%) for the 2BT selection, and 7% (5%) for the 3B selection. The likelihood procedure described in Section 6 accounts for NP contributions to all control regions in a coherent manner.

Systematic uncertainties are summarized in Table 5. We consider the systematic uncertainty associated with MC closure, evaluated as described in Section 5.1. The closure is evaluated separately for the nominal combined top-quark and W+jets simulated sample, with the W+jets cross section increased by 50% and the single-top-quark cross section by 100%, and with the W+jets cross section decreased by 50% and the single-top-quark cross section by 100% (these variations account for uncertainties on the relative cross sections; they are based on the uncertainties of the NLO calculations and on comparisons between data and simulation). We take the largest closure discrepancy as the uncertainty. We also consider the systematic uncertainty associated with subtraction of the QCD- and $Z \to \nu\bar{\nu}$-background estimates in the SB region, evaluated by varying these estimates by their uncertainties. The systematic uncertainty associated with other backgrounds is evaluated by varying the MC-based background estimates in the SB region by their uncertainties, which we assume to be $\pm 100\%$ for these small terms. A final systematic uncertainty accounts for the uncertainty on the trigger efficiency.

5.4 Top-quark and W+jets background ($E_{\mathrm{T}}^{\mathrm{miss}}$-reweighting)

We perform a second, complementary evaluation of the top-quark and W+jets background, which we refer to as the $E_{\mathrm{T}}^{\mathrm{miss}}$-reweighting method. The $E_{\mathrm{T}}^{\mathrm{miss}}$ distribution is determined separately for each of the three principal top-quark and W+jets background categories:

1. top-quark or W+jets events in which exactly one W boson decays into an e or μ, or into a τ that decays into an e or μ, while the other W boson (if any) decays hadronically;
2. top-quark or W+jets events in which exactly one W boson decays into a hadronically decaying τ, while the other W boson (if any) decays hadronically;
3. $t\bar{t}$ events in which both W bosons decay into an e, μ or τ, with the τ decaying either leptonically or hadronically.

For the 1BL selection, these three categories represent, respectively, approximately 44%, 49%, and 7% of the total expected background from top-quark and W+jets events, as determined from simulation.

5.4.1 Single e or μ events: category 1

Category 1 top-quark and W+jets background is evaluated with the SL data control sample introduced in Section 5.3. To relate event yields in the SL and SIG samples, we use constraints derived from knowledge of the W-boson polarization. The polarization of the W boson governs the angular distribution of leptons in the W boson rest frame. Because forward-going leptons are boosted to higher momentum, and backward-going leptons to lower momentum, the W-boson polarization is directly related to the lepton momentum spectrum in the laboratory frame. W-boson polarization is predicted to high precision in the SM, with calculations carried out to the next-to-next-to-leading order for $t\bar{t}$ events [33] and to NLO for W+jets events [34]. The results of these calculations are consistent with measurements [35–38].

To construct a distribution sensitive to the W-boson polarization in $W \to \ell\overline{\nu}$ (ℓ = e, μ) events (we include $W \to \tau\overline{\nu} \to \ell\overline{\nu}\nu\overline{\nu}$ events in this category), we calculate the angle $\Delta\theta_T$ between the direction of the W boson in the laboratory frame and the direction of the e or μ in the W boson rest frame, all defined in the transverse plane. The p_T of the W boson is given by the vector sum of the E_T^{miss} and charged lepton p_T vectors. When $\Delta\theta_T$ is small, the charged lepton is produced along the p_T direction of the W boson, typically resulting in a high-p_T charged lepton and a low-p_T neutrino (and therefore low E_T^{miss}) in the laboratory frame. Such events usually appear in the SL sample. Conversely, when $\Delta\theta_T$ is large, the charged lepton (neutrino) has lower (higher) p_T, typically leading to larger E_T^{miss}, a charged lepton that fails our e or μ identification criteria, and an event that appears as background in the signal samples.

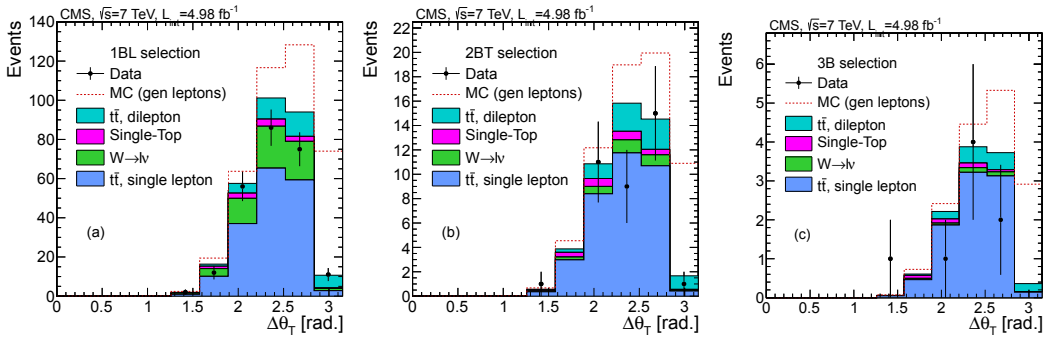

Figure 12: The distributions of $\Delta\theta_T$ for events with a single e or μ for the (a) 1BL, (b) 2BT, and (c) 3B selection criteria except with a loosened E_T^{miss} restriction for (b) as described in the text. The stacked, filled histograms show simulated predictions for events in the SL sample. The dashed histogram shows the corresponding simulated prediction in the limit of perfect charged lepton reconstruction. The simulated results are normalized as in Fig. 2.

Figure 12 shows the distribution of $\Delta\theta_T$ in data and simulation for SL events selected with the 1BL, 2BT, and 3B criteria, except a looser E_T^{miss} requirement ($E_T^{miss} > 250$ GeV) is used for the 2BT region to reduce statistical fluctuations. These results can be compared to those expected in the limit of perfect charged lepton reconstruction, indicated by the dashed histograms in Fig. 12, which show the corresponding simulated predictions, including simulation of the detector, for top-quark and W+jets events with a single $W \to \ell\nu$ decay, where the e or μ needs only to be present at the generator level. The difference between the dashed histogram and the sum of the histograms with exactly one true e or μ found in the event represents $W \to \ell\nu$ events in which the e or μ is either not reconstructed or does not meet the selection criteria of Section 3.

To estimate the E_T^{miss} distribution of category 1 events, we measure the E_T^{miss} distribution of SL events in bins of $\Delta\theta_T$. The E_T^{miss} distribution for each bin is then multiplied by an MC

Table 6: The relative systematic uncertainties (%) for the $E_{\mathrm{T}}^{\mathrm{miss}}$-reweighting estimate of the top-quark and W+jets background, for category 1 (category 2) events.

	1BL	1BT	2BL	2BT	3B
$\sigma(\mathrm{W} \to \ell\nu)/\sigma(\mathrm{t\bar{t}})$ ratio	0.1 (0.7)	3.3 (3.9)	0.1 (0.3)	0.2 (0.3)	0.6 (0.3)
Lepton efficiency	2.0 (2.0)	2.0 (2.9)	2.0 (2.0)	2.0 (2.2)	2.0 (2.0)
Top-quark p_{T} spectrum	0.1 (2.2)	6.8 (0.7)	0.6 (3.2)	1.6 (0.7)	1.6 (2.7)
Jet energy scale	1.6 (3.0)	5.0 (5.2)	1.7 (2.1)	1.2 (4.9)	1.1 (4.1)
Jet energy resolution	0.2 (0)	0.4 (1.6)	0.2 (0.2)	0.5 (0.4)	0.3 (0.2)
b-tagging efficiency	0.2 (0.4)	1.0 (2.8)	0.4 (0.6)	0.5 (0.5)	0.3 (0.4)
MC closure	10 (4.7)	55 (29)	12 (5.1)	17 (16)	21 (6.6)
τ visible energy	— (1.5)	— (3.1)	— (1.9)	— (2.0)	— (2.1)
Total	10 (6.5)	56 (30)	12 (7.0)	17 (17)	21 (8.7)

scale factor, determined as follows. The numerator equals the difference between the total yield from single-lepton processes (the dashed histograms in Fig. 12) and the subset of those events that enter the SL sample, both determined for that bin. The denominator equals the corresponding number of events that appear in the SL sample from all sources. The definition of the denominator therefore corresponds to the SL observable in data. The normalization of the $E_{\mathrm{T}}^{\mathrm{miss}}$ distribution in each $\Delta\theta_{\mathrm{T}}$ bin is thus given by the corresponding measured yield, corrected by a scale factor that accounts for the e or μ acceptance and reconstruction efficiency. The corrected $E_{\mathrm{T}}^{\mathrm{miss}}$ spectra from the different $\Delta\theta_{\mathrm{T}}$ bins are summed to provide the total $E_{\mathrm{T}}^{\mathrm{miss}}$ distribution for category 1 events.

Systematic uncertainties are summarized in Table 6. To evaluate a systematic uncertainty associated with the relative $\mathrm{t\bar{t}}$ and W+jets cross sections, we vary the W+jets cross section by $\pm 50\%$. From studies of $\mathrm{Z} \to \ell^+\ell^-$ events, the systematic uncertainty associated with the lepton reconstruction efficiency is determined to be 2%. A systematic uncertainty associated with the top-quark p_{T} spectrum is evaluated by varying the W-boson p_{T} distribution in the simulated $\mathrm{t\bar{t}}$ sample. In these variations, the number of events in the upper 10% of the distribution changes by two standard deviations of the corresponding result in data. The systematic uncertainties associated with the jet energy scale, jet energy resolution, and b-tagging efficiency are evaluated as described in Section 7. A systematic uncertainty to account for MC closure is evaluated as described in Section 5.3.

5.4.2 $\tau \to$ hadrons: category 2

Category 2 top-quark and W+jets background is evaluated using a single-muon data control sample. The muon in the event is replaced with a simulated hadronically decaying τ (a τ jet) of the same momentum. To account for the addition of the τ jet, the initial selection criteria are less restrictive than those of the nominal analysis. We require two or more jets, $E_{\mathrm{T}}^{\mathrm{miss}} > 100\,\mathrm{GeV}$, and do not place restrictions on H_{T} or $\Delta\hat{\phi}_{\mathrm{min}}$. To ensure compatibility with the triggers used to define this single-muon control sample, the minimum muon p_{T} is set to 25 GeV, and the muon isolation requirement is also more stringent than the nominal criterion of Section 3.

The visible energy fraction of the τ jet, namely its visible energy divided by its p_{T} value, is determined by sampling p_{T}-dependent MC distributions ("response templates") of the τ visible energy distribution, for a given underlying value of τ lepton p_{T}. The τ jet visible energy is added to the event. The modified event is then subjected to our standard signal region selection criteria. A normalization factor derived from simulation accounts for the relative rates of category 2 and single-muon control sample events.

Table 7: The SM background estimates from the procedures of Sections 5.1-5.4 in comparison with the observed number of events in data. The first uncertainties are statistical and the second systematic. For the total SM estimates, we give the results based both on the nominal and $E_{\mathrm{T}}^{\mathrm{miss}}$-reweighting methods to evaluate the top-quark and W+jets background.

	1BL	1BT	2BL	2BT	3B
QCD	$28 \pm 3 \pm 12$	$0.0 \pm 0.2 \pm 0.3$	$4.7 \pm 1.3 \pm 2.8$	$0.8 \pm 0.4 \pm 1.2$	$1.0 \pm 0.5 \pm 0.5$
$Z \to \nu\bar{\nu}$	$154 \pm 20 \pm 32$	$2.4 \pm 1.9 \pm 0.5$	$32 \pm 5 \pm 20$	$6.2 \pm 2.0 \pm 3.9$	$4.7 \pm 1.3 \pm 6.5$
top quark & W+jets:					
nominal	$337 \pm 30 \pm 63$	$6.5 \pm 3.3 \pm 1.8$	$123 \pm 17 \pm 19$	$22.8 \pm 6.9 \pm 5.5$	$8.8 \pm 4.0 \pm 1.8$
$E_{\mathrm{T}}^{\mathrm{miss}}$-reweighting	$295 \pm 16 \pm 17$	$4.0 \pm 1.2 \pm 1.5$	$116 \pm 8 \pm 8$	$19.8 \pm 2.5 \pm 2.2$	$13.6 \pm 3.2 \pm 1.2$
Total SM:					
nominal	$519 \pm 36 \pm 72$	$8.9 \pm 3.8 \pm 1.9$	$159 \pm 18 \pm 28$	$29.8 \pm 7.2 \pm 6.8$	$14.4 \pm 4.2 \pm 6.8$
$E_{\mathrm{T}}^{\mathrm{miss}}$-reweighting	$477 \pm 26 \pm 38$	$6.4 \pm 2.3 \pm 1.6$	$153 \pm 10 \pm 22$	$26.8 \pm 3.2 \pm 4.6$	$19.3 \pm 3.5 \pm 6.6$
Data	478	11	146	45	22

The same systematic uncertainties are considered as for category 1 events. In addition, we evaluate an uncertainty for the τ jet visible energy by varying the τ energy scale by $\pm 3\%$ [39]. Systematic uncertainties are summarized in Table 6.

5.4.3 $t\bar{t}$ dilepton events: category 3

The contribution of category 3 top-quark and W+jets background events is determined using dilepton data control samples. When both leptons are electrons or both are muons, or when one is an electron and the other a muon (where the e or μ can either be from a W boson or τ decay), we use simulated predictions to describe the shape of the $E_{\mathrm{T}}^{\mathrm{miss}}$ distribution. The normalization is derived from data, by measuring the number of dilepton events that satisfy loosened selection criteria for each class of events (ee, $\mu\mu$, or eμ) individually. The measured value is multiplied by an MC scale factor, defined by the number of corresponding $t\bar{t}$ dilepton events that satisfy the final selection criteria divided by the number that satisfy the loosened criteria.

When one or both of the leptons is a hadronically decaying τ, we apply a procedure similar to that described for category 2 events. Data control samples of eμ+jets and $\mu\mu$+jets events are selected with the loosened criteria of Section 5.4.2. One or both muons is replaced by a τ-jet using MC response templates. The signal sample selection criteria are applied to the modified events, and the resulting $E_{\mathrm{T}}^{\mathrm{miss}}$ distributions normalized by scaling the number of events in the respective control samples with factors derived from MC simulation.

The $E_{\mathrm{T}}^{\mathrm{miss}}$ distributions of all six dilepton categories are summed to provide the total category 3 prediction. A systematic uncertainty is evaluated based on MC closure in the manner described in Section 5.1.

5.5 Summary of the data-based background estimates

A summary of the background estimates is given in Table 7. The results from the three categories of Section 5.4 are summed to provide the total $E_{\mathrm{T}}^{\mathrm{miss}}$-reweighting top-quark and W+jets prediction. The estimates from the $E_{\mathrm{T}}^{\mathrm{miss}}$-reweighting method are seen to be consistent with those from the nominal method and to yield smaller uncertainties. Note that there are statistical correlations between the nominal and $E_{\mathrm{T}}^{\mathrm{miss}}$-reweighting methods because they both make use of the SIG-SL region of Fig. 11. However, the nominal method relies on the SB and SB-SL regions of Fig. 11, while the $E_{\mathrm{T}}^{\mathrm{miss}}$-reweighting method does not. The $E_{\mathrm{T}}^{\mathrm{miss}}$-reweighting method makes use of MC scale factors and data selected with lepton-based triggers (for category 2 and 3 events), while the nominal method does not. Furthermore, the systematic uncertainties of the

two methods are largely uncorrelated (compare Tables 5 and 6).

The data are generally in good agreement with the SM expectations. However, for 2BT, the data lie 1.1 and 2.2 standard deviations (σ) above the predictions (including systematic uncertainties) for the nominal and $E_{\mathrm{T}}^{\mathrm{miss}}$-reweighting methods, respectively. For 3B, the corresponding deviations are 1.2σ and 0.7σ. Since these deviations are not significant, we do not consider them further.

As an illustration, Fig. 13 presents the background predictions in comparison to data for the 1BL, 2BT, and 3B selections. These results are based on the nominal top-quark and W+jets background estimate.

6 Likelihood analysis

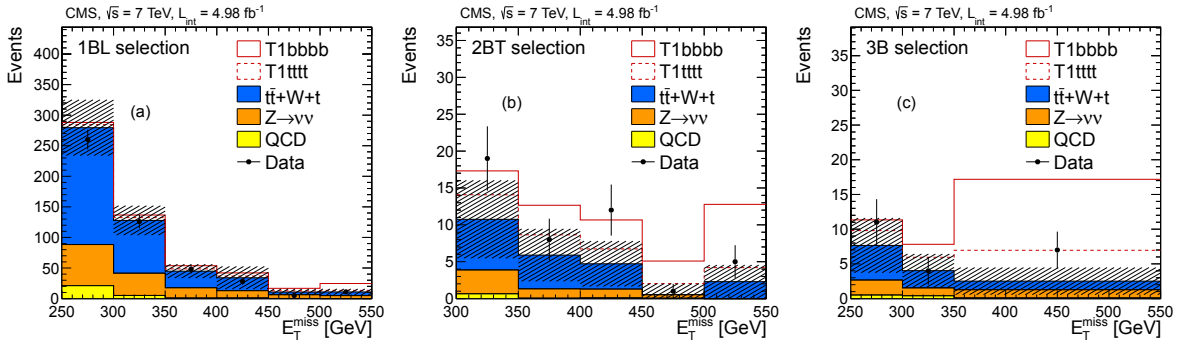

Figure 13: The data-based SM background predictions for $E_{\mathrm{T}}^{\mathrm{miss}}$ in the (a) 1BL, (b) 2BT, and (c) 3B signal regions in comparison to data. The top-quark and W+jets estimate is based on the nominal method. The hatched bands show the total uncertainty on the prediction, including systematic uncertainties. The uncertainties are correlated between bins. The open histograms show the expectations for the T1bbbb (solid line) and T1tttt (dashed line) NP models, both with $m_{\tilde{\mathrm{g}}} = 925\,\mathrm{GeV}$, $m_{\mathrm{LSP}} = 100\,\mathrm{GeV}$, and normalization to NLO+NLL.

We perform a global likelihood fit that simultaneously determines the SM background and yield of a NP model, using the background estimation techniques of Section 5. The likelihood analysis allows us to treat the SM backgrounds in a more unified manner than is possible through the collection of individual results in Table 7. Furthermore, it allows us to account for NP contributions to the control regions ("signal contamination"), as well as to the signal region, in a comprehensive and consistent manner.

It is difficult to account for signal contamination using the $E_{\mathrm{T}}^{\mathrm{miss}}$-reweighting method, in contrast to the nominal method. Therefore, signal contamination is evaluated for the nominal method only. Of the two NP scenarios we consider, one of them, the T1tttt model, exhibits non-negligible contamination of the SL samples, while the other, the T1bbbb model, does not. Since the T1bbbb model does not exhibit significant signal contamination, we employ both the nominal- and $E_{\mathrm{T}}^{\mathrm{miss}}$-reweighting-based likelihood fits for this model. For the T1tttt model, we employ only the likelihood fit based on the nominal method.

For the nominal method, the data are divided into 11 mutually exclusive bins, corresponding to the 11 observables listed in Table 8, where each "observable" corresponds to the number of data events recorded for that bin. Note that the SB-SL events of Fig. 11 are divided into two components, one for electrons (denoted SB–Se) and the other for muons (denoted SB–Sμ), because their trigger efficiencies and uncertainties differ. Similarly, the reconstruction efficiencies

Table 8: The observables (number of data events) of the likelihood analysis for the nominal method, representing the signal region and ten control regions. The seven observables listed in the upper portion of the table are subject to contributions from the signal model in our analysis. The E_T^{miss} SB region corresponds to $150 < E_T^{miss} < 250$ GeV while the SIG regions correspond to the E_T^{miss} regions listed in Table 1. The low $\Delta\hat{\phi}_{min}$ region corresponds to $\Delta\hat{\phi}_{min} < 4.0$.

SIG	Standard selection, E_T^{miss} SIG region
SB	Standard selection, E_T^{miss} SB region
SIG–LDP	Standard selection, E_T^{miss} SIG/low $\Delta\hat{\phi}_{min}$ region
SB–LDP	Standard selection, E_T^{miss} SB/low $\Delta\hat{\phi}_{min}$ region
SIG–SL	Single-lepton selection, E_T^{miss} SIG region
SB–Se	Single-electron selection, E_T^{miss} SB region
SB–Sμ	Single-muon selection, E_T^{miss} SB region
SIG–ee	$Z \to e^+e^-$ selection, E_T^{miss} SIG region
SB–ee	$Z \to e^+e^-$ selection, E_T^{miss} SB region
SIG–$\mu\mu$	$Z \to \mu^+\mu^-$ selection, E_T^{miss} SIG region
SB–$\mu\mu$	$Z \to \mu^+\mu^-$ selection, E_T^{miss} SB region

of $Z \to e^+e^-$ and $Z \to \mu^+\mu^-$ events differ, so we divide the $Z \to \ell^+\ell^-$ events of Section 5.2 according to the lepton flavor. We further divide the $Z \to \ell^+\ell^-$ events according to whether they appear in the sideband ($150 < E_T^{miss} < 250$ GeV) or signal regions (Table 1) of E_T^{miss}. The four $Z \to \ell^+\ell^-$ samples are denoted SIG-ee and SIG-$\mu\mu$ for events in the signal regions, and SB-ee and SB-$\mu\mu$ for events in the sideband region.

The likelihood model provides a prediction for the mean expected value of each observable in terms of the parameters of the signal and background components. The likelihood function is the product of 11 Poisson probability density functions, one for each observable, β distributions [40] that parametrize efficiencies and acceptances, and β' distributions [40] that account for systematic uncertainties and uncertainties on external parameters. (External parameters include such quantities as the acceptance $\mathcal{A}$ and scale factors between the samples with loose and nominal b-tagging requirements discussed in Section 5.2.) The new physics scenarios considered here can contribute significantly to the seven observables listed in the upper portion of Table 8. In our model, the relative contributions of NP to these seven observables are taken from the NP model under consideration. The NP yield in the SIG bin is a free parameter. The NP contributions to the other six bins thus depend on the NP yield in the SIG bin.

Analogous procedures are used to define the likelihood function for the E_T^{miss}-reweighting method, with simplifications since there is no SB region in this case.

The likelihood function is used to set limits on NP models. Upper limits at 95% confidence level (CL) are evaluated taking into account the effects of variation of the external parameters and their correlations. All upper limits are determined using a modified frequentist technique (CL_s) [41, 42].

7 Limits on the T1bbbb and T1tttt models

Simulated T1bbbb and T1tttt event samples are generated for a range of gluino and LSP masses using PYTHIA, with $m_{LSP} < m_{\tilde{g}}$. For increased efficiency when performing scans over the SMS parameter space (see below), we base simulation of the CMS detector response on the fast simulation program [43], accounting for modest differences observed with respect to the GEANT4 simulation.

Table 9: The relative systematic uncertainties (%) for the signal efficiency of the T1bbbb SMS model with $m_{\tilde{g}} = 925\,\text{GeV}$ and $m_{\text{LSP}} = 100\,\text{GeV}$.

	1BL	1BT	2BL	2BT	3B
Jet energy scale	2.1	11	2.1	3.5	1.9
Unclustered energy	0.2	0.8	0.2	0.2	0.2
Jet energy resolution	1.0	2.0	1.0	1.0	1.0
Pileup	1.0	1.0	1.0	1.0	1.0
b-jet tagging efficiency	0.8	0.9	3.8	3.9	9.0
Trigger efficiency	3.6	3.6	3.6	3.6	3.6
Parton distribution functions	0.4	1.6	0.4	0.7	0.5
Anomalous $E_{\text{T}}^{\text{miss}}$	1.0	1.0	1.0	1.0	1.0
Lepton veto	3.0	3.0	3.0	3.0	3.0
Luminosity	2.2	2.2	2.2	2.2	2.2
Total uncertainty	5.9	12	7.0	7.6	11

Systematic uncertainties on signal efficiency are summarized in Table 9, using the T1bbbb benchmark model as an example. A systematic uncertainty associated with the jet energy scale is evaluated by varying this scale by its p_{T}- and η-dependent uncertainties. A systematic uncertainty associated with unclustered energy is evaluated by varying the transverse energy in an event that is not clustered into a physics object by $\pm 10\%$. The systematic uncertainties associated with the correction to the jet energy resolution, the pileup reweighting method mentioned in Section 3, the b-jet tagging efficiency scale factor, and the trigger efficiency, are evaluated by varying the respective quantities by their uncertainties. The uncertainty for the trigger efficiency includes a 2.5% uncertainty for the plateau efficiency. Systematic uncertainties associated with the parton distribution functions are evaluated following the recommendations of Ref. [44]. The systematic uncertainty associated with anomalous $E_{\text{T}}^{\text{miss}}$ values, caused by beam background and reconstruction effects, is 1%. The systematic uncertainty associated with the lepton veto is determined from studies of $Z \to \ell^+\ell^-$ events in data to be 3.0%. The uncertainty in the luminosity determination is 2.2% [45].

We determine 95% CL upper limits on the SMS cross sections as a function of the gluino and LSP masses. Using the NLO+NLL cross section as a reference, we also evaluate 95% CL exclusion curves. The jet energy scale, unclustered energy, parton distribution function, and b-jet tagging efficiency uncertainties are evaluated for each scan point. Other uncertainties are fixed to the values in Table 9. For each choice of gluino and LSP mass, we use the combination of the top-quark and W+jets background estimation method, and the signal selection (Table 1), that provides the best expected limit. We do not include results for points near the $m_{\tilde{g}} = m_{\text{LSP}}$ diagonal because of neglected uncertainties from initial-state radiation (ISR), which are large in this region. Specifically, we remove from consideration any point for which the signal efficiency changes by more than 50% when the ISR radiation in PYTHIA is (effectively) turned off.

For the T1bbbb model, the $E_{\text{T}}^{\text{miss}}$-reweighting method is always found to provide the best expected result: we therefore use this method to determine the T1bbbb limits. The $E_{\text{T}}^{\text{miss}}$-reweighting method incorporates an additional constraint compared to the nominal method, namely the normalization of the SM prediction for the $E_{\text{T}}^{\text{miss}}$ distribution from the SIG-SL sample (Fig. 11), and not merely the $E_{\text{T}}^{\text{miss}}$ distribution shape. As a consequence, it has greater discrimination power against NP scenarios.

The results for T1bbbb are shown in Fig. 14(a). The 1BT selection is found to provide the best expected result in the bottom right corner of the distribution, corresponding to the region of large gluino-LSP mass splitting. The 2BT selection is best for the swath roughly parallel to the

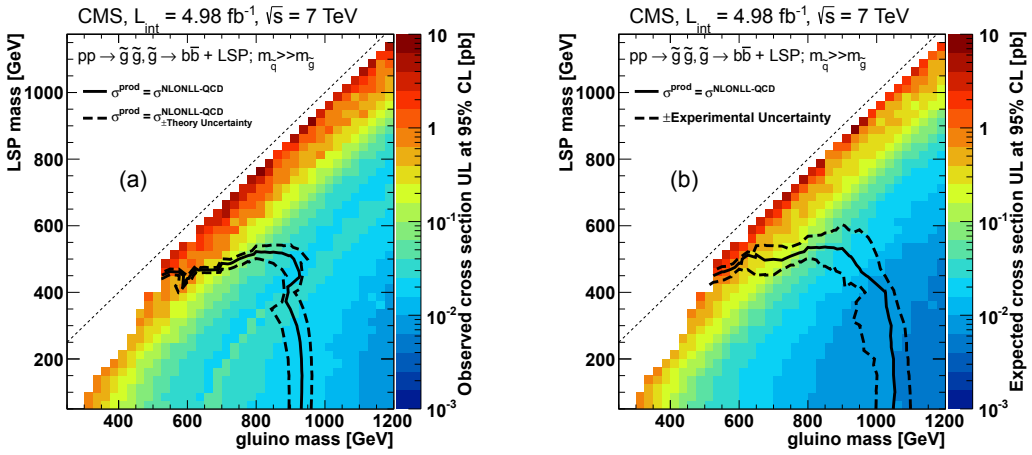

Figure 14: (a) The 95% CL observed cross section upper limits (UL) for the T1bbbb SMS model, based on the $E_{\mathrm{T}}^{\mathrm{miss}}$-reweighting method to evaluate the top-quark and W+jets background. For each point, the selection that provides the best expected cross section limit is used. The solid contour shows the 95% CL exclusion limits on the gluino and LSP masses using the NLO+NLL cross section for new physics. The dashed contours represent the theory uncertainties. (b) The corresponding expected limits. The dashed contours represent the uncertainties on the SM background estimates.

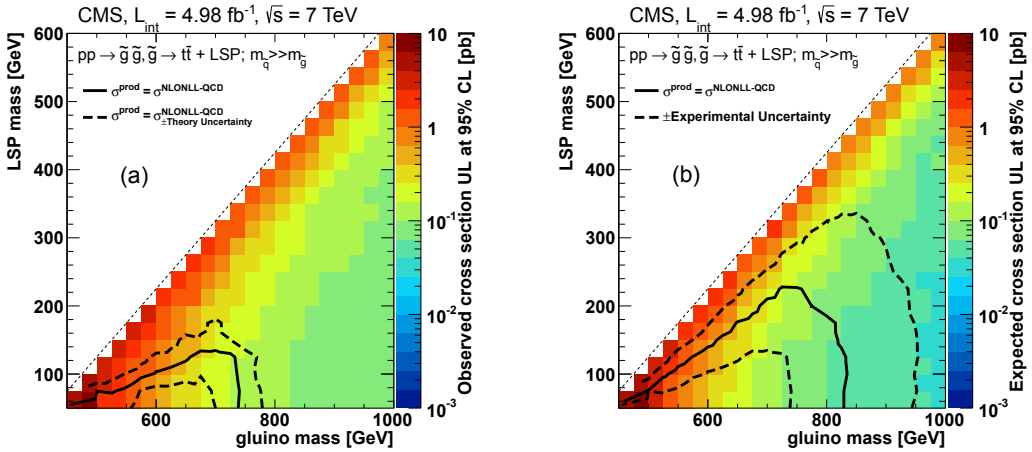

Figure 15: (a) The 95% CL observed cross section upper limits (UL) for the T1tttt SMS model, based on the nominal method to evaluate the top-quark and W+jets background. For each point, the selection that provides the best expected cross section limit is used (the best selection is virtually always 3B). The solid contour shows the 95% CL exclusion limits on the gluino and LSP masses using the NLO+NLL cross section for new physics. The dashed contours represent the theory uncertainties. (b) The corresponding expected limits. The dashed contours represent the uncertainties on the SM background estimates.

diagonal defined by gluino masses between around 650 and 900 GeV along the bottom edge of the plot. The 3B selection is generally best elsewhere. The solid contour shows the 95% CL exclusion curve for the reference cross section. The zigzagging structure around $m_{\tilde{g}} = 900\,\text{GeV}$, $m_{\text{LSP}} = 450\,\text{GeV}$ is due to the transition from the region where 3B is the best expected selection to that where 2BT is best, in conjunction with the slight excess observed in data for the 2BT selection in comparison with the SM prediction for the $E_{\text{T}}^{\text{miss}}$-reweighting method (Section 5.5). The dashed contours represent the results when the reference cross section is varied by the theory uncertainty [46]. Our results improve those of Ref. [7] for large LSP mass values. For example, for gluino masses around 800 GeV, we extend the exclusion of the reference cross section from an LSP mass of about 400 GeV [7] to about 500 GeV, where these numerical values are given by the observed results minus the one standard deviation theory uncertainties.

Fig. 14(b) shows the best expected results for the T1bbbb model. In this case the dashed contours represent the results when the SM background estimates (Table 7) are varied by their uncertainties.

Even with the selection requirement against ISR events described above, the effect of ISR events can be significant for T1bbbb scenarios that lie within three or four cell widths of the diagonal, where the size of a cell is indicated by the small boxes visible near the diagonal in Fig. 14. We do not account for the effect of ISR for these scenarios. However, for gluino masses less than around 500 GeV, and for points more than three to four cell widths from the diagonal, the effect of ISR is negligible for the points that are retained. This includes the entire exclusion region for the NLO+NLL reference cross section.

The corresponding results for the T1tttt model are presented in Fig. 15. Our T1tttt results are based on the nominal top-quark and W+jets background estimation method for the reason stated in Section 6. In this case, the best expected selection is essentially always 3B. Note that the observed limits for T1tttt, shown in Fig 15(a), are not as stringent as the expected limits, shown in Fig 15(b), because of the slight excess of data events in the 3B sample for the nominal method, compared to the SM expectation (Table 7).

8 Summary

In this paper, we present a search for an anomalous rate of events with three or more jets, at least one, two, or three tagged bottom-quark jets, no identified, isolated leptons, and large missing transverse energy $E_{\text{T}}^{\text{miss}}$. The study is based on a sample of proton-proton collision data collected at $\sqrt{s} = 7\,\text{TeV}$ with the CMS detector at the LHC during 2011, corresponding to an integrated luminosity of $4.98\,\text{fb}^{-1}$. The principal standard model backgrounds, arising from top-quark, W+jets, Z+jets, and QCD-multijet events, are evaluated from data. We introduce a variable $\Delta\hat{\phi}_{\text{min}}$ that allows us to address the QCD-multijet background with a simple approach. The top-quark and W+jets background is evaluated with two complementary methods, which yield consistent results. In the $E_{\text{T}}^{\text{miss}}$-reweighting method to evaluate the top-quark and W+jets background, we introduce a technique based on the W polarization in $\text{t}\bar{\text{t}}$ and W+jets events. Our analysis is performed in a likelihood framework in order to account for backgrounds, and for new physics contamination of the control regions, in a unified and consistent manner.

We find no evidence for a significant excess of events beyond the expectations of the standard model and set limits on new physics in the context of the b-jet-rich T1bbbb and T1tttt simplified model spectra, in which new strongly interacting particles decay to two b-quark jets, or two t-quark jets, plus an undetected particle. For the T1bbbb scenario, our results improve on those of Ref. [7] for large LSP masses.

Acknowledgements

We congratulate our colleagues in the CERN accelerator departments for the excellent performance of the LHC machine. We thank the technical and administrative staff at CERN and other CMS institutes. This work was supported by the Austrian Federal Ministry of Science and Research; the Belgian Fonds de la Recherche Scientifique, and Fonds voor Wetenschappelijk Onderzoek; the Brazilian Funding Agencies (CNPq, CAPES, FAPERJ, and FAPESP); the Bulgarian Ministry of Education and Science; CERN; the Chinese Academy of Sciences, Ministry of Science and Technology, and National Natural Science Foundation of China; the Colombian Funding Agency (COLCIENCIAS); the Croatian Ministry of Science, Education and Sport; the Research Promotion Foundation, Cyprus; the Ministry of Education and Research, Recurrent financing contract SF0690030s09 and European Regional Development Fund, Estonia; the Academy of Finland, Finnish Ministry of Education and Culture, and Helsinki Institute of Physics; the Institut National de Physique Nucléaire et de Physique des Particules / CNRS, and Commissariat à l'Énergie Atomique et aux Énergies Alternatives / CEA, France; the Bundesministerium für Bildung und Forschung, Deutsche Forschungsgemeinschaft, and Helmholtz-Gemeinschaft Deutscher Forschungszentren, Germany; the General Secretariat for Research and Technology, Greece; the National Scientific Research Foundation, and National Office for Research and Technology, Hungary; the Department of Atomic Energy and the Department of Science and Technology, India; the Institute for Studies in Theoretical Physics and Mathematics, Iran; the Science Foundation, Ireland; the Istituto Nazionale di Fisica Nucleare, Italy; the Korean Ministry of Education, Science and Technology and the World Class University program of NRF, Korea; the Lithuanian Academy of Sciences; the Mexican Funding Agencies (CINVESTAV, CONACYT, SEP, and UASLP-FAI); the Ministry of Science and Innovation, New Zealand; the Pakistan Atomic Energy Commission; the Ministry of Science and Higher Education and the National Science Centre, Poland; the Fundação para a Ciência e a Tecnologia, Portugal; JINR (Armenia, Belarus, Georgia, Ukraine, Uzbekistan); the Ministry of Education and Science of the Russian Federation, the Federal Agency of Atomic Energy of the Russian Federation, Russian Academy of Sciences, and the Russian Foundation for Basic Research; the Ministry of Science and Technological Development of Serbia; the Secretaría de Estado de Investigación, Desarrollo e Innovación and Programa Consolider-Ingenio 2010, Spain; the Swiss Funding Agencies (ETH Board, ETH Zurich, PSI, SNF, UniZH, Canton Zurich, and SER); the National Science Council, Taipei; the Scientific and Technical Research Council of Turkey, and Turkish Atomic Energy Authority; the Science and Technology Facilities Council, UK; the US Department of Energy, and the US National Science Foundation.

Individuals have received support from the Marie-Curie programme and the European Research Council (European Union); the Leventis Foundation; the A. P. Sloan Foundation; the Alexander von Humboldt Foundation; the Belgian Federal Science Policy Office; the Fonds pour la Formation à la Recherche dans l'Industrie et dans l'Agriculture (FRIA-Belgium); the Agentschap voor Innovatie door Wetenschap en Technologie (IWT-Belgium); the Council of Science and Industrial Research, India; the Compagnia di San Paolo (Torino); and the HOMING PLUS programme of Foundation for Polish Science, cofinanced from European Union, Regional Development Fund.

References

[1] G. R. Farrar and P. Fayet, "Phenomenology of the production, decay, and detection of new hadronic states associated with supersymmetry", *Phys. Lett. B* **76** (1978) 575, doi:10.1016/0370-2693(78)90858-4.

[2] J. Wess and B. Zumino, "Supergauge transformations in four dimensions", *Nucl. Phys. B* **70** (1974) 39, doi:10.1016/0550-3213(74)90355-1.

[3] S. P. Martin, "A supersymmetry primer", (1997). arXiv:hep-ph/9709356.

[4] CMS Collaboration, "Search for supersymmetry in events with b jets and missing transverse energy at the LHC", *J. High Energy Phys.* **07** (2011) 113, doi:10.1007/JHEP07(2011)113.

[5] ATLAS Collaboration, "Search for supersymmetry in pp collisions at $\sqrt{s} = 7$ TeV in final states with missing transverse momentum and b jets", *Phys. Lett. B* **701** (2011) 398, doi:10.1016/j.physletb.2011.06.015.

[6] ATLAS Collaboration, "Search for supersymmetry in pp collisions at $\sqrt{s} = 7$ TeV in final states with missing transverse momentum and b-jets with the ATLAS Detector", *Phys. Rev. D* **85** (2012) 112006, doi:10.1103/PhysRevD.85.112006.

[7] CMS Collaboration, "Search for supersymmetry in hadronic final states using M_{T2} in pp collisions at $\sqrt{s} = 7$ TeV", (2012). arXiv:1207.1798. In press in J. High Energy Phys.

[8] ATLAS Collaboration, "Search for top and bottom squarks from gluino pair production in final states with missing transverse energy and at least three b-jets with the ATLAS detector", (2012). arXiv:1207.4686. Submitted to Eur. Phys. Journal C.

[9] N. Arkani-Hamed et al., "MARMOSET: The path from LHC data to the new standard model via on-shell effective theories", (2007). arXiv:hep-ph/0703088.

[10] J. Alwall, P. C. Schuster, and N. Toro, "Simplified models for a first characterization of new physics at the LHC", *Phys. Rev. D* **79** (2009) 075020, doi:10.1103/PhysRevD.79.075020.

[11] J. Alwall et al., "Model-independent jets plus missing energy searches", *Phys. Rev. D* **79** (2009) 015005, doi:10.1103/PhysRevD.79.015005.

[12] D. Alves et al., "Simplified models for LHC new physics searches", (2011). arXiv:1105.2838.

[13] W. Beenakker et al., "Squark and gluino production at hadron colliders", *Nucl. Phys. B* **492** (1997) 51, doi:10.1016/S0550-3213(97)00084-9.

[14] A. Kulesza and L. Motyka, "Threshold resummation for squark-antisquark and gluino-pair production at the LHC", *Phys. Rev. Lett.* **102** (2009) 111802, doi:10.1103/PhysRevLett.102.111802.

[15] A. Kulesza and L. Motyka, "Soft gluon resummation for the production of gluino-gluino and squark-antisquark pairs at the LHC", *Phys. Rev. D* **80** (2009) 095004, doi:10.1103/PhysRevD.80.095004.

[16] W. Beenakker et al., "Soft-gluon resummation for squark and gluino hadroproduction", *J. High Energy Phys.* **12** (2009) 041, doi:10.1088/1126-6708/2009/12/041.

[17] W. Beenakker et al., "Squark and gluino hadroproduction", *Int. J. Mod. Phys. A* **26** (2011) 2637, doi:10.1142/S0217751X11053560.

[18] CMS Collaboration, "The CMS experiment at the CERN LHC", *Journal of Instrum.* **03** (2008) S08004, doi:10.1088/1748-0221/3/08/S08004.

[19] CMS Collaboration, "Particle flow event reconstruction in CMS and performance for jets, taus and $E_{\mathrm{T}}^{\mathrm{miss}}$", CMS Physics Analysis Summary CMS-PAS-PFT-09-001, (2009).

[20] M. Cacciari, G. P. Salam, and G. Soyez, "The anti-k_t jet clustering algorithm", *J. High Energy Phys.* **04** (2008) 063, doi:10.1088/1126-6708/2008/04/063.

[21] CMS Collaboration, "Determination of jet energy calibration and transverse momentum resolution in CMS", *Journal of Instrum.* **06** (2011) 11002, doi:10.1088/1748-0221/6/11/P11002.

[22] CMS Collaboration, "Tracking and primary vertex results in first 7 TeV collisions", CMS Physics Analysis Summary CMS-PAS-TRK-10-005, (2010).

[23] CMS Collaboration, "Electron reconstruction and identification at $\sqrt{s} = 7$ TeV", CMS Physics Analysis Summary CMS-PAS-EGM-10-004, (2010).

[24] CMS Collaboration, "Performance of CMS muon reconstruction in pp collision events at $\sqrt{s} = 7$ TeV", (2012). arXiv:1206.4071. Submitted to Journal of Instrum.

[25] CMS Collaboration, "b-jet identification in the CMS experiment", CMS Physics Analysis Summary CMS-PAS-BTV-11-004, (2012).

[26] J. Alwall et al., "MadGraph5: going beyond", *J. High Energy Phys.* **06** (2011) 128, doi:10.1007/JHEP06(2011)128.

[27] S. Frixione, P. Nason, and C. Oleari, "Matching NLO QCD computations with parton shower simulations: the POWHEG method", *J. High Energy Phys.* **11** (2007) 070, doi:10.1088/1126-6708/2007/11/070.

[28] T. Sjöstrand, S. Mrenna, and P. Skands, "PYTHIA 6.4 physics and manual", *J. High Energy Phys.* **05** (2006) 026, doi:10.1088/1126-6708/2006/05/026.

[29] J. Pumplin et al., "New generation of parton distributions with uncertainties from global QCD analysis", *J. High Energy Phys.* **07** (2002) 12, doi:10.1088/1126-6708/2002/07/012.

[30] S. Agostinelli et al., "GEANT4—a simulation toolkit", *Nucl. Instr. and Meth. A* **506** (2003) 250, doi:10.1016/S0168-9002(03)01368-8.

[31] CMS Collaboration, "Measurement of the $\mathrm{t\bar{t}}$ production cross section in pp collisions at 7 TeV in lepton + jets events using b-quark jet identification", *Phys. Rev. D* **84** (2011) 092004, doi:10.1103/PhysRevD.84.092004.

[32] K. Nakamura et al., "Review of particle physics", *J. Phys. G* **37** (2010) 075021, doi:10.1088/0954-3899/37/7A/075021.

[33] A. Czarnecki, J. G. Körner, and J. H. Piclum, "Helicity fractions of W bosons from top quark decays at NNLO in QCD", *Phys. Rev. D* **81** (2010) 111503, doi:10.1103/PhysRevD.81.111503.

[34] Z. Bern et al., "Left-handed W bosons at the LHC", *Phys. Rev. D* **84** (2011) 034008, doi:10.1103/PhysRevD.84.034008.

[35] CDF Collaboration, "Measurement of W boson polarization in top quark decay in $\mathrm{p\bar{p}}$ collisions at $\sqrt{s} = 1.96$ TeV", *Phys. Rev. Lett.* **105** (2010) 042002, doi:10.1103/PhysRevLett.105.042002.

[36] D0 Collaboration, "Measurement of the W boson helicity in top quark decays using 5.4 fb^{-1} of $p\bar{p}$ collision data", *Phys. Rev. D* **83** (2011) 032009, doi:10.1103/PhysRevD.83.032009.

[37] CMS Collaboration, "Measurement of the polarization of W bosons with large transverse momentum in W+jets events at the LHC", *Phys. Rev. Lett.* **107** (2011) 021802, doi:10.1103/PhysRevLett.107.021802.

[38] ATLAS Collaboration, "Measurement of the W boson polarization in top quark decays with the ATLAS detector", *J. High Energy Phys.* **06** (2012) 088, doi:10.1007/JHEP06(2012)088.

[39] CMS Collaboration, "Performance of τ-lepton reconstruction and identification in CMS", *Journal of Instrum.* **07** (2012) P01001, doi:10.1088/1748-0221/7/01/P01001.

[40] N. L. Johnson, S. Kotz, and N. N. Balakrishnan, "Continuous Univariate Distributions", volume 2. Wiley Interscience, 1995.

[41] T. Junk, "Confidence level computation for combining searches with small statistics", *Nucl. Instr. and Meth. A* **434** (1999) 435, doi:10.1016/S0168-9002(99)00498-2.

[42] A. L. Read, "Presentation of search results: the CL_s technique", *J. Phys. G* **28** (2002) 2693, doi:10.1088/0954-3899/28/10/313.

[43] CMS Collaboration, "Comparison of the fast simulation of CMS with the first LHC data", CMS Detector Performance Summary CMS-DP-2010-039, (2010).

[44] M. Botje et al., "The PDF4LHC working group interim recommendations", (2011). arXiv:1101.0538.

[45] CMS Collaboration, "Absolute calibration of the luminosity measurement at CMS: winter 2012 update", CMS Physics Analysis Summary CMS-PAS-SMP-12-008, (2012).

[46] M. Krämer et al., "Supersymmetry production cross sections in pp collisions at $\sqrt{s} = 7$ TeV", (2012). arXiv:1206.2892.

A The CMS Collaboration

Yerevan Physics Institute, Yerevan, Armenia
S. Chatrchyan, V. Khachatryan, A.M. Sirunyan, A. Tumasyan

Institut für Hochenergiephysik der OeAW, Wien, Austria
W. Adam, E. Aguilo, T. Bergauer, M. Dragicevic, J. Erö, C. Fabjan[1], M. Friedl, R. Frühwirth[1], V.M. Ghete, J. Hammer, N. Hörmann, J. Hrubec, M. Jeitler[1], W. Kiesenhofer, V. Knünz, M. Krammer[1], I. Krätschmer, D. Liko, I. Mikulec, M. Pernicka†, B. Rahbaran, C. Rohringer, H. Rohringer, R. Schöfbeck, J. Strauss, A. Taurok, W. Waltenberger, G. Walzel, E. Widl, C.-E. Wulz[1]

National Centre for Particle and High Energy Physics, Minsk, Belarus
V. Mossolov, N. Shumeiko, J. Suarez Gonzalez

Universiteit Antwerpen, Antwerpen, Belgium
M. Bansal, S. Bansal, T. Cornelis, E.A. De Wolf, X. Janssen, S. Luyckx, L. Mucibello, S. Ochesanu, B. Roland, R. Rougny, M. Selvaggi, Z. Staykova, H. Van Haevermaet, P. Van Mechelen, N. Van Remortel, A. Van Spilbeeck

Vrije Universiteit Brussel, Brussel, Belgium
F. Blekman, S. Blyweert, J. D'Hondt, R. Gonzalez Suarez, A. Kalogeropoulos, M. Maes, A. Olbrechts, W. Van Doninck, P. Van Mulders, G.P. Van Onsem, I. Villella

Université Libre de Bruxelles, Bruxelles, Belgium
B. Clerbaux, G. De Lentdecker, V. Dero, A.P.R. Gay, T. Hreus, A. Léonard, P.E. Marage, T. Reis, L. Thomas, G. Vander Marcken, C. Vander Velde, P. Vanlaer, J. Wang

Ghent University, Ghent, Belgium
V. Adler, K. Beernaert, A. Cimmino, S. Costantini, G. Garcia, M. Grunewald, B. Klein, J. Lellouch, A. Marinov, J. Mccartin, A.A. Ocampo Rios, D. Ryckbosch, N. Strobbe, F. Thyssen, M. Tytgat, P. Verwilligen, S. Walsh, E. Yazgan, N. Zaganidis

Université Catholique de Louvain, Louvain-la-Neuve, Belgium
S. Basegmez, G. Bruno, R. Castello, L. Ceard, C. Delaere, T. du Pree, D. Favart, L. Forthomme, A. Giammanco[2], J. Hollar, V. Lemaitre, J. Liao, O. Militaru, C. Nuttens, D. Pagano, A. Pin, K. Piotrzkowski, N. Schul, J.M. Vizan Garcia

Université de Mons, Mons, Belgium
N. Beliy, T. Caebergs, E. Daubie, G.H. Hammad

Centro Brasileiro de Pesquisas Fisicas, Rio de Janeiro, Brazil
G.A. Alves, M. Correa Martins Junior, D. De Jesus Damiao, T. Martins, M.E. Pol, M.H.G. Souza

Universidade do Estado do Rio de Janeiro, Rio de Janeiro, Brazil
W.L. Aldá Júnior, W. Carvalho, A. Custódio, E.M. Da Costa, C. De Oliveira Martins, S. Fonseca De Souza, D. Matos Figueiredo, L. Mundim, H. Nogima, V. Oguri, W.L. Prado Da Silva, A. Santoro, L. Soares Jorge, A. Sznajder

Instituto de Fisica Teorica, Universidade Estadual Paulista, Sao Paulo, Brazil
T.S. Anjos[3], C.A. Bernardes[3], F.A. Dias[4], T.R. Fernandez Perez Tomei, E. M. Gregores[3], C. Lagana, F. Marinho, P.G. Mercadante[3], S.F. Novaes, Sandra S. Padula

Institute for Nuclear Research and Nuclear Energy, Sofia, Bulgaria
V. Genchev[5], P. Iaydjiev[5], S. Piperov, M. Rodozov, S. Stoykova, G. Sultanov, V. Tcholakov, R. Trayanov, M. Vutova

University of Sofia, Sofia, Bulgaria
A. Dimitrov, R. Hadjiiska, V. Kozhuharov, L. Litov, B. Pavlov, P. Petkov

Institute of High Energy Physics, Beijing, China
J.G. Bian, G.M. Chen, H.S. Chen, C.H. Jiang, D. Liang, S. Liang, X. Meng, J. Tao, J. Wang, X. Wang, Z. Wang, H. Xiao, M. Xu, J. Zang, Z. Zhang

State Key Lab. of Nucl. Phys. and Tech., Peking University, Beijing, China
C. Asawatangtrakuldee, Y. Ban, Y. Guo, W. Li, S. Liu, Y. Mao, S.J. Qian, H. Teng, D. Wang, L. Zhang, W. Zou

Universidad de Los Andes, Bogota, Colombia
C. Avila, J.P. Gomez, B. Gomez Moreno, A.F. Osorio Oliveros, J.C. Sanabria

Technical University of Split, Split, Croatia
N. Godinovic, D. Lelas, R. Plestina[6], D. Polic, I. Puljak[5]

University of Split, Split, Croatia
Z. Antunovic, M. Kovac

Institute Rudjer Boskovic, Zagreb, Croatia
V. Brigljevic, S. Duric, K. Kadija, J. Luetic, S. Morovic

University of Cyprus, Nicosia, Cyprus
A. Attikis, M. Galanti, G. Mavromanolakis, J. Mousa, C. Nicolaou, F. Ptochos, P.A. Razis

Charles University, Prague, Czech Republic
M. Finger, M. Finger Jr.

Academy of Scientific Research and Technology of the Arab Republic of Egypt, Egyptian Network of High Energy Physics, Cairo, Egypt
Y. Assran[7], S. Elgammal[8], A. Ellithi Kamel[9], S. Khalil[8], M.A. Mahmoud[10], A. Radi[11,12]

National Institute of Chemical Physics and Biophysics, Tallinn, Estonia
M. Kadastik, M. Müntel, M. Raidal, L. Rebane, A. Tiko

Department of Physics, University of Helsinki, Helsinki, Finland
P. Eerola, G. Fedi, M. Voutilainen

Helsinki Institute of Physics, Helsinki, Finland
J. Härkönen, A. Heikkinen, V. Karimäki, R. Kinnunen, M.J. Kortelainen, T. Lampén, K. Lassila-Perini, S. Lehti, T. Lindén, P. Luukka, T. Mäenpää, T. Peltola, E. Tuominen, J. Tuominiemi, E. Tuovinen, D. Ungaro, L. Wendland

Lappeenranta University of Technology, Lappeenranta, Finland
K. Banzuzi, A. Karjalainen, A. Korpela, T. Tuuva

DSM/IRFU, CEA/Saclay, Gif-sur-Yvette, France
M. Besancon, S. Choudhury, M. Dejardin, D. Denegri, B. Fabbro, J.L. Faure, F. Ferri, S. Ganjour, A. Givernaud, P. Gras, G. Hamel de Monchenault, P. Jarry, E. Locci, J. Malcles, L. Millischer, A. Nayak, J. Rander, A. Rosowsky, I. Shreyber, M. Titov

Laboratoire Leprince-Ringuet, Ecole Polytechnique, IN2P3-CNRS, Palaiseau, France
S. Baffioni, F. Beaudette, L. Benhabib, L. Bianchini, M. Bluj[13], C. Broutin, P. Busson, C. Charlot, N. Daci, T. Dahms, L. Dobrzynski, R. Granier de Cassagnac, M. Haguenauer, P. Miné, C. Mironov, I.N. Naranjo, M. Nguyen, C. Ochando, P. Paganini, D. Sabes, R. Salerno, Y. Sirois, C. Veelken, A. Zabi

Institut Pluridisciplinaire Hubert Curien, Université de Strasbourg, Université de Haute Alsace Mulhouse, CNRS/IN2P3, Strasbourg, France
J.-L. Agram[14], J. Andrea, D. Bloch, D. Bodin, J.-M. Brom, M. Cardaci, E.C. Chabert, C. Collard, E. Conte[14], F. Drouhin[14], C. Ferro, J.-C. Fontaine[14], D. Gelé, U. Goerlach, P. Juillot, A.-C. Le Bihan, P. Van Hove

Centre de Calcul de l'Institut National de Physique Nucleaire et de Physique des Particules, CNRS/IN2P3, Villeurbanne, France, Villeurbanne, France
F. Fassi, D. Mercier

Université de Lyon, Université Claude Bernard Lyon 1, CNRS-IN2P3, Institut de Physique Nucléaire de Lyon, Villeurbanne, France
S. Beauceron, N. Beaupere, O. Bondu, G. Boudoul, J. Chasserat, R. Chierici[5], D. Contardo, P. Depasse, H. El Mamouni, J. Fay, S. Gascon, M. Gouzevitch, B. Ille, T. Kurca, M. Lethuillier, L. Mirabito, S. Perries, V. Sordini, Y. Tschudi, P. Verdier, S. Viret

Institute of High Energy Physics and Informatization, Tbilisi State University, Tbilisi, Georgia
Z. Tsamalaidze[15]

RWTH Aachen University, I. Physikalisches Institut, Aachen, Germany
G. Anagnostou, C. Autermann, S. Beranek, M. Edelhoff, L. Feld, N. Heracleous, O. Hindrichs, R. Jussen, K. Klein, J. Merz, A. Ostapchuk, A. Perieanu, F. Raupach, J. Sammet, S. Schael, D. Sprenger, H. Weber, B. Wittmer, V. Zhukov[16]

RWTH Aachen University, III. Physikalisches Institut A, Aachen, Germany
M. Ata, J. Caudron, E. Dietz-Laursonn, D. Duchardt, M. Erdmann, R. Fischer, A. Güth, T. Hebbeker, C. Heidemann, K. Hoepfner, D. Klingebiel, P. Kreuzer, M. Merschmeyer, A. Meyer, M. Olschewski, P. Papacz, H. Pieta, H. Reithler, S.A. Schmitz, L. Sonnenschein, J. Steggemann, D. Teyssier, M. Weber

RWTH Aachen University, III. Physikalisches Institut B, Aachen, Germany
M. Bontenackels, V. Cherepanov, Y. Erdogan, G. Flügge, H. Geenen, M. Geisler, W. Haj Ahmad, F. Hoehle, B. Kargoll, T. Kress, Y. Kuessel, A. Nowack, L. Perchalla, O. Pooth, P. Sauerland, A. Stahl

Deutsches Elektronen-Synchrotron, Hamburg, Germany
M. Aldaya Martin, J. Behr, W. Behrenhoff, U. Behrens, M. Bergholz[17], A. Bethani, K. Borras, A. Burgmeier, A. Cakir, L. Calligaris, A. Campbell, E. Castro, F. Costanza, D. Dammann, C. Diez Pardos, G. Eckerlin, D. Eckstein, G. Flucke, A. Geiser, I. Glushkov, P. Gunnellini, S. Habib, J. Hauk, G. Hellwig, H. Jung, M. Kasemann, P. Katsas, C. Kleinwort, H. Kluge, A. Knutsson, M. Krämer, D. Krücker, E. Kuznetsova, W. Lange, W. Lohmann[17], B. Lutz, R. Mankel, I. Marfin, M. Marienfeld, I.-A. Melzer-Pellmann, A.B. Meyer, J. Mnich, A. Mussgiller, S. Naumann-Emme, O. Novgorodova, J. Olzem, H. Perrey, A. Petrukhin, D. Pitzl, A. Raspereza, P.M. Ribeiro Cipriano, C. Riedl, E. Ron, M. Rosin, J. Salfeld-Nebgen, R. Schmidt[17], T. Schoerner-Sadenius, N. Sen, A. Spiridonov, M. Stein, R. Walsh, C. Wissing

University of Hamburg, Hamburg, Germany
V. Blobel, J. Draeger, H. Enderle, J. Erfle, U. Gebbert, M. Görner, T. Hermanns, R.S. Höing, K. Kaschube, G. Kaussen, H. Kirschenmann, R. Klanner, J. Lange, B. Mura, F. Nowak, T. Peiffer, N. Pietsch, D. Rathjens, C. Sander, H. Schettler, P. Schleper, E. Schlieckau, A. Schmidt, M. Schröder, T. Schum, M. Seidel, V. Sola, H. Stadie, G. Steinbrück, J. Thomsen, L. Vanelderen

Institut für Experimentelle Kernphysik, Karlsruhe, Germany
C. Barth, J. Berger, C. Böser, T. Chwalek, W. De Boer, A. Descroix, A. Dierlamm, M. Feindt, M. Guthoff[5], C. Hackstein, F. Hartmann, T. Hauth[5], M. Heinrich, H. Held, K.H. Hoffmann, S. Honc, I. Katkov[16], J.R. Komaragiri, P. Lobelle Pardo, D. Martschei, S. Mueller, Th. Müller, M. Niegel, A. Nürnberg, O. Oberst, A. Oehler, J. Ott, G. Quast, K. Rabbertz, F. Ratnikov, N. Ratnikova, S. Röcker, A. Scheurer, F.-P. Schilling, G. Schott, H.J. Simonis, F.M. Stober, D. Troendle, R. Ulrich, J. Wagner-Kuhr, S. Wayand, T. Weiler, M. Zeise

Institute of Nuclear Physics "Demokritos", Aghia Paraskevi, Greece
G. Daskalakis, T. Geralis, S. Kesisoglou, A. Kyriakis, D. Loukas, I. Manolakos, A. Markou, C. Markou, C. Mavrommatis, E. Ntomari

University of Athens, Athens, Greece
L. Gouskos, T.J. Mertzimekis, A. Panagiotou, N. Saoulidou

University of Ioánnina, Ioánnina, Greece
I. Evangelou, C. Foudas, P. Kokkas, N. Manthos, I. Papadopoulos, V. Patras

KFKI Research Institute for Particle and Nuclear Physics, Budapest, Hungary
G. Bencze, C. Hajdu, P. Hidas, D. Horvath[18], F. Sikler, V. Veszpremi, G. Vesztergombi[19]

Institute of Nuclear Research ATOMKI, Debrecen, Hungary
N. Beni, S. Czellar, J. Molnar, J. Palinkas, Z. Szillasi

University of Debrecen, Debrecen, Hungary
J. Karancsi, P. Raics, Z.L. Trocsanyi, B. Ujvari

Panjab University, Chandigarh, India
S.B. Beri, V. Bhatnagar, N. Dhingra, R. Gupta, M. Kaur, M.Z. Mehta, N. Nishu, L.K. Saini, A. Sharma, J. Singh

University of Delhi, Delhi, India
Ashok Kumar, Arun Kumar, S. Ahuja, A. Bhardwaj, B.C. Choudhary, S. Malhotra, M. Naimuddin, K. Ranjan, V. Sharma, R.K. Shivpuri

Saha Institute of Nuclear Physics, Kolkata, India
S. Banerjee, S. Bhattacharya, S. Dutta, B. Gomber, Sa. Jain, Sh. Jain, R. Khurana, S. Sarkar, M. Sharan

Bhabha Atomic Research Centre, Mumbai, India
A. Abdulsalam, R.K. Choudhury, D. Dutta, S. Kailas, V. Kumar, P. Mehta, A.K. Mohanty[5], L.M. Pant, P. Shukla

Tata Institute of Fundamental Research - EHEP, Mumbai, India
T. Aziz, S. Ganguly, M. Guchait[20], M. Maity[21], G. Majumder, K. Mazumdar, G.B. Mohanty, B. Parida, K. Sudhakar, N. Wickramage

Tata Institute of Fundamental Research - HECR, Mumbai, India
S. Banerjee, S. Dugad

Institute for Research in Fundamental Sciences (IPM), Tehran, Iran
H. Arfaei, H. Bakhshiansohi[22], S.M. Etesami[23], A. Fahim[22], M. Hashemi, H. Hesari, A. Jafari[22], M. Khakzad, M. Mohammadi Najafabadi, S. Paktinat Mehdiabadi, B. Safarzadeh[24], M. Zeinali[23]

INFN Sezione di Bari [a], Università di Bari [b], Politecnico di Bari [c], Bari, Italy
M. Abbrescia[a,b], L. Barbone[a,b], C. Calabria[a,b,5], S.S. Chhibra[a,b], A. Colaleo[a], D. Creanza[a,c],

N. De Filippis[a,c,5], M. De Palma[a,b], L. Fiore[a], G. Iaselli[a,c], L. Lusito[a,b], G. Maggi[a,c], M. Maggi[a], B. Marangelli[a,b], S. My[a,c], S. Nuzzo[a,b], N. Pacifico[a,b], A. Pompili[a,b], G. Pugliese[a,c], G. Selvaggi[a,b], L. Silvestris[a], G. Singh[a,b], R. Venditti[a,b], G. Zito[a]

INFN Sezione di Bologna [a], Università di Bologna [b], Bologna, Italy
G. Abbiendi[a], A.C. Benvenuti[a], D. Bonacorsi[a,b], S. Braibant-Giacomelli[a,b], L. Brigliadori[a,b], P. Capiluppi[a,b], A. Castro[a,b], F.R. Cavallo[a], M. Cuffiani[a,b], G.M. Dallavalle[a], F. Fabbri[a], A. Fanfani[a,b], D. Fasanella[a,b,5], P. Giacomelli[a], C. Grandi[a], L. Guiducci[a,b], S. Marcellini[a], G. Masetti[a], M. Meneghelli[a,b,5], A. Montanari[a], F.L. Navarria[a,b], F. Odorici[a], A. Perrotta[a], F. Primavera[a,b], A.M. Rossi[a,b], T. Rovelli[a,b], G. Siroli[a,b], R. Travaglini[a,b]

INFN Sezione di Catania [a], Università di Catania [b], Catania, Italy
S. Albergo[a,b], G. Cappello[a,b], M. Chiorboli[a,b], S. Costa[a,b], R. Potenza[a,b], A. Tricomi[a,b], C. Tuve[a,b]

INFN Sezione di Firenze [a], Università di Firenze [b], Firenze, Italy
G. Barbagli[a], V. Ciulli[a,b], C. Civinini[a], R. D'Alessandro[a,b], E. Focardi[a,b], S. Frosali[a,b], E. Gallo[a], S. Gonzi[a,b], M. Meschini[a], S. Paoletti[a], G. Sguazzoni[a], A. Tropiano[a]

INFN Laboratori Nazionali di Frascati, Frascati, Italy
L. Benussi, S. Bianco, S. Colafranceschi[25], F. Fabbri, D. Piccolo

INFN Sezione di Genova [a], Università di Genova [b], Genova, Italy
P. Fabbricatore[a], R. Musenich[a], S. Tosi[a,b]

INFN Sezione di Milano-Bicocca [a], Università di Milano-Bicocca [b], Milano, Italy
A. Benaglia[a,b], F. De Guio[a,b], L. Di Matteo[a,b,5], S. Fiorendi[a,b], S. Gennai[a,5], A. Ghezzi[a,b], S. Malvezzi[a], R.A. Manzoni[a,b], A. Martelli[a,b], A. Massironi[a,b,5], D. Menasce[a], L. Moroni[a], M. Paganoni[a,b], D. Pedrini[a], S. Ragazzi[a,b], N. Redaelli[a], S. Sala[a], T. Tabarelli de Fatis[a,b]

INFN Sezione di Napoli [a], Università di Napoli "Federico II" [b], Napoli, Italy
S. Buontempo[a], C.A. Carrillo Montoya[a], N. Cavallo[a,26], A. De Cosa[a,b,5], O. Dogangun[a,b], F. Fabozzi[a,26], A.O.M. Iorio[a], L. Lista[a], S. Meola[a,27], M. Merola[a,b], P. Paolucci[a,5]

INFN Sezione di Padova [a], Università di Padova [b], Università di Trento (Trento) [c], Padova, Italy
P. Azzi[a], N. Bacchetta[a,5], D. Bisello[a,b], A. Branca[a,b,5], R. Carlin[a,b], P. Checchia[a], T. Dorigo[a], U. Dosselli[a], F. Gasparini[a,b], U. Gasparini[a,b], A. Gozzelino[a], K. Kanishchev[a,c], S. Lacaprara[a], I. Lazzizzera[a,c], M. Margoni[a,b], A.T. Meneguzzo[a,b], J. Pazzini[a,b], N. Pozzobon[a,b], P. Ronchese[a,b], F. Simonetto[a,b], E. Torassa[a], M. Tosi[a,b,5], S. Vanini[a,b], P. Zotto[a,b], G. Zumerle[a,b]

INFN Sezione di Pavia [a], Università di Pavia [b], Pavia, Italy
M. Gabusi[a,b], S.P. Ratti[a,b], C. Riccardi[a,b], P. Torre[a,b], P. Vitulo[a,b]

INFN Sezione di Perugia [a], Università di Perugia [b], Perugia, Italy
M. Biasini[a,b], G.M. Bilei[a], L. Fanò[a,b], P. Lariccia[a,b], A. Lucaroni[a,b,5], G. Mantovani[a,b], M. Menichelli[a], A. Nappi[a,b†], F. Romeo[a,b], A. Saha[a], A. Santocchia[a,b], A. Spiezia[a,b], S. Taroni[a,b]

INFN Sezione di Pisa [a], Università di Pisa [b], Scuola Normale Superiore di Pisa [c], Pisa, Italy
P. Azzurri[a,c], G. Bagliesi[a], T. Boccali[a], G. Broccolo[a,c], R. Castaldi[a], R.T. D'Agnolo[a,c,5], R. Dell'Orso[a], F. Fiori[a,b,5], L. Foà[a,c], A. Giassi[a], A. Kraan[a], F. Ligabue[a,c], T. Lomtadze[a], L. Martini[a,28], A. Messineo[a,b], F. Palla[a], A. Rizzi[a,b], A.T. Serban[a,29], P. Spagnolo[a], P. Squillacioti[a,5], R. Tenchini[a], G. Tonelli[a,b], A. Venturi[a], P.G. Verdini[a]

INFN Sezione di Roma [a], Università di Roma "La Sapienza" [b], Roma, Italy
L. Barone[a,b], F. Cavallari[a], D. Del Re[a,b], M. Diemoz[a], C. Fanelli, M. Grassi[a,b,5], E. Longo[a,b],

P. Meridiani[a,5], F. Micheli[a,b], S. Nourbakhsh[a,b], G. Organtini[a,b], R. Paramatti[a], S. Rahatlou[a,b], M. Sigamani[a], L. Soffi[a,b]

INFN Sezione di Torino [a], Università di Torino [b], Università del Piemonte Orientale (Novara) [c], Torino, Italy
N. Amapane[a,b], R. Arcidiacono[a,c], S. Argiro[a,b], M. Arneodo[a,c], C. Biino[a], N. Cartiglia[a], M. Costa[a,b], P. De Remigis[a], N. Demaria[a], C. Mariotti[a,5], S. Maselli[a], E. Migliore[a,b], V. Monaco[a,b], M. Musich[a,5], M.M. Obertino[a,c], N. Pastrone[a], M. Pelliccioni[a], A. Potenza[a,b], A. Romero[a,b], R. Sacchi[a,b], A. Solano[a,b], A. Staiano[a], A. Vilela Pereira[a]

INFN Sezione di Trieste [a], Università di Trieste [b], Trieste, Italy
S. Belforte[a], V. Candelise[a,b], F. Cossutti[a], G. Della Ricca[a,b], B. Gobbo[a], M. Marone[a,b,5], D. Montanino[a,b,5], A. Penzo[a], A. Schizzi[a,b]

Kangwon National University, Chunchon, Korea
S.G. Heo, T.Y. Kim, S.K. Nam

Kyungpook National University, Daegu, Korea
S. Chang, D.H. Kim, G.N. Kim, D.J. Kong, H. Park, S.R. Ro, D.C. Son, T. Son

Chonnam National University, Institute for Universe and Elementary Particles, Kwangju, Korea
J.Y. Kim, Zero J. Kim, S. Song

Korea University, Seoul, Korea
S. Choi, D. Gyun, B. Hong, M. Jo, H. Kim, T.J. Kim, K.S. Lee, D.H. Moon, S.K. Park

University of Seoul, Seoul, Korea
M. Choi, J.H. Kim, C. Park, I.C. Park, S. Park, G. Ryu

Sungkyunkwan University, Suwon, Korea
Y. Cho, Y. Choi, Y.K. Choi, J. Goh, M.S. Kim, E. Kwon, B. Lee, J. Lee, S. Lee, H. Seo, I. Yu

Vilnius University, Vilnius, Lithuania
M.J. Bilinskas, I. Grigelionis, M. Janulis, A. Juodagalvis

Centro de Investigacion y de Estudios Avanzados del IPN, Mexico City, Mexico
H. Castilla-Valdez, E. De La Cruz-Burelo, I. Heredia-de La Cruz, R. Lopez-Fernandez, R. Magaña Villalba, J. Martínez-Ortega, A. Sánchez-Hernández, L.M. Villasenor-Cendejas

Universidad Iberoamericana, Mexico City, Mexico
S. Carrillo Moreno, F. Vazquez Valencia

Benemerita Universidad Autonoma de Puebla, Puebla, Mexico
H.A. Salazar Ibarguen

Universidad Autónoma de San Luis Potosí, San Luis Potosí, Mexico
E. Casimiro Linares, A. Morelos Pineda, M.A. Reyes-Santos

University of Auckland, Auckland, New Zealand
D. Krofcheck

University of Canterbury, Christchurch, New Zealand
A.J. Bell, P.H. Butler, R. Doesburg, S. Reucroft, H. Silverwood

National Centre for Physics, Quaid-I-Azam University, Islamabad, Pakistan
M. Ahmad, M.H. Ansari, M.I. Asghar, H.R. Hoorani, S. Khalid, W.A. Khan, T. Khurshid, S. Qazi, M.A. Shah, M. Shoaib

National Centre for Nuclear Research, Swierk, Poland
H. Bialkowska, B. Boimska, T. Frueboes, R. Gokieli, M. Górski, M. Kazana, K. Nawrocki, K. Romanowska-Rybinska, M. Szleper, G. Wrochna, P. Zalewski

Institute of Experimental Physics, Faculty of Physics, University of Warsaw, Warsaw, Poland
G. Brona, K. Bunkowski, M. Cwiok, W. Dominik, K. Doroba, A. Kalinowski, M. Konecki, J. Krolikowski

Laboratório de Instrumentação e Física Experimental de Partículas, Lisboa, Portugal
N. Almeida, P. Bargassa, A. David, P. Faccioli, P.G. Ferreira Parracho, M. Gallinaro, J. Seixas, J. Varela, P. Vischia

Joint Institute for Nuclear Research, Dubna, Russia
I. Belotelov, P. Bunin, I. Golutvin, A. Kamenev, V. Karjavin, V. Konoplyanikov, G. Kozlov, A. Lanev, A. Malakhov, P. Moisenz, V. Palichik, V. Perelygin, M. Savina, S. Shmatov, V. Smirnov, A. Volodko, A. Zarubin

Petersburg Nuclear Physics Institute, Gatchina (St Petersburg), Russia
S. Evstyukhin, V. Golovtsov, Y. Ivanov, V. Kim, P. Levchenko, V. Murzin, V. Oreshkin, I. Smirnov, V. Sulimov, L. Uvarov, S. Vavilov, A. Vorobyev, An. Vorobyev

Institute for Nuclear Research, Moscow, Russia
Yu. Andreev, A. Dermenev, S. Gninenko, N. Golubev, M. Kirsanov, N. Krasnikov, V. Matveev, A. Pashenkov, D. Tlisov, A. Toropin

Institute for Theoretical and Experimental Physics, Moscow, Russia
V. Epshteyn, M. Erofeeva, V. Gavrilov, M. Kossov, N. Lychkovskaya, V. Popov, G. Safronov, S. Semenov, V. Stolin, E. Vlasov, A. Zhokin

Moscow State University, Moscow, Russia
A. Belyaev, E. Boos, M. Dubinin[4], L. Dudko, A. Ershov, A. Gribushin, V. Klyukhin, O. Kodolova, I. Lokhtin, A. Markina, S. Obraztsov, M. Perfilov, S. Petrushanko, A. Popov, L. Sarycheva†, V. Savrin, A. Snigirev

P.N. Lebedev Physical Institute, Moscow, Russia
V. Andreev, M. Azarkin, I. Dremin, M. Kirakosyan, A. Leonidov, G. Mesyats, S.V. Rusakov, A. Vinogradov

State Research Center of Russian Federation, Institute for High Energy Physics, Protvino, Russia
I. Azhgirey, I. Bayshev, S. Bitioukov, V. Grishin[5], V. Kachanov, D. Konstantinov, V. Krychkine, V. Petrov, R. Ryutin, A. Sobol, L. Tourtchanovitch, S. Troshin, N. Tyurin, A. Uzunian, A. Volkov

University of Belgrade, Faculty of Physics and Vinca Institute of Nuclear Sciences, Belgrade, Serbia
P. Adzic[30], M. Djordjevic, M. Ekmedzic, D. Krpic[30], J. Milosevic

Centro de Investigaciones Energéticas Medioambientales y Tecnológicas (CIEMAT), Madrid, Spain
M. Aguilar-Benitez, J. Alcaraz Maestre, P. Arce, C. Battilana, E. Calvo, M. Cerrada, M. Chamizo Llatas, N. Colino, B. De La Cruz, A. Delgado Peris, D. Domínguez Vázquez, C. Fernandez

Bedoya, J.P. Fernández Ramos, A. Ferrando, J. Flix, M.C. Fouz, P. Garcia-Abia, O. Gonzalez Lopez, S. Goy Lopez, J.M. Hernandez, M.I. Josa, G. Merino, J. Puerta Pelayo, A. Quintario Olmeda, I. Redondo, L. Romero, J. Santaolalla, M.S. Soares, C. Willmott

Universidad Autónoma de Madrid, Madrid, Spain
C. Albajar, G. Codispoti, J.F. de Trocóniz

Universidad de Oviedo, Oviedo, Spain
H. Brun, J. Cuevas, J. Fernandez Menendez, S. Folgueras, I. Gonzalez Caballero, L. Lloret Iglesias, J. Piedra Gomez

Instituto de Física de Cantabria (IFCA), CSIC-Universidad de Cantabria, Santander, Spain
J.A. Brochero Cifuentes, I.J. Cabrillo, A. Calderon, S.H. Chuang, J. Duarte Campderros, M. Felcini[31], M. Fernandez, G. Gomez, J. Gonzalez Sanchez, A. Graziano, C. Jorda, A. Lopez Virto, J. Marco, R. Marco, C. Martinez Rivero, F. Matorras, F.J. Munoz Sanchez, T. Rodrigo, A.Y. Rodríguez-Marrero, A. Ruiz-Jimeno, L. Scodellaro, I. Vila, R. Vilar Cortabitarte

CERN, European Organization for Nuclear Research, Geneva, Switzerland
D. Abbaneo, E. Auffray, G. Auzinger, M. Bachtis, P. Baillon, A.H. Ball, D. Barney, J.F. Benitez, C. Bernet[6], G. Bianchi, P. Bloch, A. Bocci, A. Bonato, C. Botta, H. Breuker, T. Camporesi, G. Cerminara, T. Christiansen, J.A. Coarasa Perez, D. D'Enterria, A. Dabrowski, A. De Roeck, S. Di Guida, M. Dobson, N. Dupont-Sagorin, A. Elliott-Peisert, B. Frisch, W. Funk, G. Georgiou, M. Giffels, D. Gigi, K. Gill, D. Giordano, M. Giunta, F. Glege, R. Gomez-Reino Garrido, P. Govoni, S. Gowdy, R. Guida, M. Hansen, P. Harris, C. Hartl, J. Harvey, B. Hegner, A. Hinzmann, V. Innocente, P. Janot, K. Kaadze, E. Karavakis, K. Kousouris, P. Lecoq, Y.-J. Lee, P. Lenzi, C. Lourenço, N. Magini, T. Mäki, M. Malberti, L. Malgeri, M. Mannelli, L. Masetti, F. Meijers, S. Mersi, E. Meschi, R. Moser, M.U. Mozer, M. Mulders, P. Musella, E. Nesvold, T. Orimoto, L. Orsini, E. Palencia Cortezon, E. Perez, L. Perrozzi, A. Petrilli, A. Pfeiffer, M. Pierini, M. Pimiä, D. Piparo, G. Polese, L. Quertenmont, A. Racz, W. Reece, J. Rodrigues Antunes, G. Rolandi[32], C. Rovelli[33], M. Rovere, H. Sakulin, F. Santanastasio, C. Schäfer, C. Schwick, I. Segoni, S. Sekmen, A. Sharma, P. Siegrist, P. Silva, M. Simon, P. Sphicas[34], D. Spiga, A. Tsirou, G.I. Veres[19], J.R. Vlimant, H.K. Wöhri, S.D. Worm[35], W.D. Zeuner

Paul Scherrer Institut, Villigen, Switzerland
W. Bertl, K. Deiters, W. Erdmann, K. Gabathuler, R. Horisberger, Q. Ingram, H.C. Kaestli, S. König, D. Kotlinski, U. Langenegger, F. Meier, D. Renker, T. Rohe, J. Sibille[36]

Institute for Particle Physics, ETH Zurich, Zurich, Switzerland
L. Bäni, P. Bortignon, M.A. Buchmann, B. Casal, N. Chanon, A. Deisher, G. Dissertori, M. Dittmar, M. Donegà, M. Dünser, J. Eugster, K. Freudenreich, C. Grab, D. Hits, P. Lecomte, W. Lustermann, A.C. Marini, P. Martinez Ruiz del Arbol, N. Mohr, F. Moortgat, C. Nägeli[37], P. Nef, F. Nessi-Tedaldi, F. Pandolfi, L. Pape, F. Pauss, M. Peruzzi, F.J. Ronga, M. Rossini, L. Sala, A.K. Sanchez, A. Starodumov[38], B. Stieger, M. Takahashi, L. Tauscher†, A. Thea, K. Theofilatos, D. Treille, C. Urscheler, R. Wallny, H.A. Weber, L. Wehrli

Universität Zürich, Zurich, Switzerland
C. Amsler, V. Chiochia, S. De Visscher, C. Favaro, M. Ivova Rikova, B. Millan Mejias, P. Otiougova, P. Robmann, H. Snoek, S. Tupputi, M. Verzetti

National Central University, Chung-Li, Taiwan
Y.H. Chang, K.H. Chen, C.M. Kuo, S.W. Li, W. Lin, Z.K. Liu, Y.J. Lu, D. Mekterovic, A.P. Singh, R. Volpe, S.S. Yu

National Taiwan University (NTU), Taipei, Taiwan
P. Bartalini, P. Chang, Y.H. Chang, Y.W. Chang, Y. Chao, K.F. Chen, C. Dietz, U. Grundler, W.-S. Hou, Y. Hsiung, K.Y. Kao, Y.J. Lei, R.-S. Lu, D. Majumder, E. Petrakou, X. Shi, J.G. Shiu, Y.M. Tzeng, X. Wan, M. Wang

Cukurova University, Adana, Turkey
A. Adiguzel, M.N. Bakirci[39], S. Cerci[40], C. Dozen, I. Dumanoglu, E. Eskut, S. Girgis, G. Gokbulut, E. Gurpinar, I. Hos, E.E. Kangal, T. Karaman, G. Karapinar[41], A. Kayis Topaksu, G. Onengut, K. Ozdemir, S. Ozturk[42], A. Polatoz, K. Sogut[43], D. Sunar Cerci[40], B. Tali[40], H. Topakli[39], L.N. Vergili, M. Vergili

Middle East Technical University, Physics Department, Ankara, Turkey
I.V. Akin, T. Aliev, B. Bilin, S. Bilmis, M. Deniz, H. Gamsizkan, A.M. Guler, K. Ocalan, A. Ozpineci, M. Serin, R. Sever, U.E. Surat, M. Yalvac, E. Yildirim, M. Zeyrek

Bogazici University, Istanbul, Turkey
E. Gülmez, B. Isildak[44], M. Kaya[45], O. Kaya[45], S. Ozkorucuklu[46], N. Sonmez[47]

Istanbul Technical University, Istanbul, Turkey
K. Cankocak

National Scientific Center, Kharkov Institute of Physics and Technology, Kharkov, Ukraine
L. Levchuk

University of Bristol, Bristol, United Kingdom
F. Bostock, J.J. Brooke, E. Clement, D. Cussans, H. Flacher, R. Frazier, J. Goldstein, M. Grimes, G.P. Heath, H.F. Heath, L. Kreczko, S. Metson, D.M. Newbold[35], K. Nirunpong, A. Poll, S. Senkin, V.J. Smith, T. Williams

Rutherford Appleton Laboratory, Didcot, United Kingdom
L. Basso[48], K.W. Bell, A. Belyaev[48], C. Brew, R.M. Brown, D.J.A. Cockerill, J.A. Coughlan, K. Harder, S. Harper, J. Jackson, B.W. Kennedy, E. Olaiya, D. Petyt, B.C. Radburn-Smith, C.H. Shepherd-Themistocleous, I.R. Tomalin, W.J. Womersley

Imperial College, London, United Kingdom
R. Bainbridge, G. Ball, R. Beuselinck, O. Buchmuller, D. Colling, N. Cripps, M. Cutajar, P. Dauncey, G. Davies, M. Della Negra, W. Ferguson, J. Fulcher, D. Futyan, A. Gilbert, A. Guneratne Bryer, G. Hall, Z. Hatherell, J. Hays, G. Iles, M. Jarvis, G. Karapostoli, L. Lyons, A.-M. Magnan, J. Marrouche, B. Mathias, R. Nandi, J. Nash, A. Nikitenko[38], A. Papageorgiou, J. Pela, M. Pesaresi, K. Petridis, M. Pioppi[49], D.M. Raymond, S. Rogerson, A. Rose, M.J. Ryan, C. Seez, P. Sharp[†], A. Sparrow, M. Stoye, A. Tapper, M. Vazquez Acosta, T. Virdee, S. Wakefield, N. Wardle, T. Whyntie

Brunel University, Uxbridge, United Kingdom
M. Chadwick, J.E. Cole, P.R. Hobson, A. Khan, P. Kyberd, D. Leggat, D. Leslie, W. Martin, I.D. Reid, P. Symonds, L. Teodorescu, M. Turner

Baylor University, Waco, USA
K. Hatakeyama, H. Liu, T. Scarborough

The University of Alabama, Tuscaloosa, USA
O. Charaf, C. Henderson, P. Rumerio

Boston University, Boston, USA
A. Avetisyan, T. Bose, C. Fantasia, A. Heister, J. St. John, P. Lawson, D. Lazic, J. Rohlf, D. Sperka, L. Sulak

Brown University, Providence, USA
J. Alimena, S. Bhattacharya, D. Cutts, A. Ferapontov, U. Heintz, S. Jabeen, G. Kukartsev, E. Laird, G. Landsberg, M. Luk, M. Narain, D. Nguyen, M. Segala, T. Sinthuprasith, T. Speer, K.V. Tsang

University of California, Davis, Davis, USA
R. Breedon, G. Breto, M. Calderon De La Barca Sanchez, S. Chauhan, M. Chertok, J. Conway, R. Conway, P.T. Cox, J. Dolen, R. Erbacher, M. Gardner, R. Houtz, W. Ko, A. Kopecky, R. Lander, T. Miceli, D. Pellett, F. Ricci-tam, B. Rutherford, M. Searle, J. Smith, M. Squires, M. Tripathi, R. Vasquez Sierra

University of California, Los Angeles, Los Angeles, USA
V. Andreev, D. Cline, R. Cousins, J. Duris, S. Erhan, P. Everaerts, C. Farrell, J. Hauser, M. Ignatenko, C. Jarvis, C. Plager, G. Rakness, P. Schlein†, P. Traczyk, V. Valuev, M. Weber

University of California, Riverside, Riverside, USA
J. Babb, R. Clare, M.E. Dinardo, J. Ellison, J.W. Gary, F. Giordano, G. Hanson, G.Y. Jeng[50], H. Liu, O.R. Long, A. Luthra, H. Nguyen, S. Paramesvaran, J. Sturdy, S. Sumowidagdo, R. Wilken, S. Wimpenny

University of California, San Diego, La Jolla, USA
W. Andrews, J.G. Branson, G.B. Cerati, S. Cittolin, D. Evans, F. Golf, A. Holzner, R. Kelley, M. Lebourgeois, J. Letts, I. Macneill, B. Mangano, S. Padhi, C. Palmer, G. Petrucciani, M. Pieri, M. Sani, V. Sharma, S. Simon, E. Sudano, M. Tadel, Y. Tu, A. Vartak, S. Wasserbaech[51], F. Würthwein, A. Yagil, J. Yoo

University of California, Santa Barbara, Santa Barbara, USA
D. Barge, R. Bellan, C. Campagnari, M. D'Alfonso, T. Danielson, K. Flowers, P. Geffert, J. Incandela, C. Justus, P. Kalavase, S.A. Koay, D. Kovalskyi, V. Krutelyov, S. Lowette, N. Mccoll, V. Pavlunin, F. Rebassoo, J. Ribnik, J. Richman, R. Rossin, D. Stuart, W. To, C. West

California Institute of Technology, Pasadena, USA
A. Apresyan, A. Bornheim, Y. Chen, E. Di Marco, J. Duarte, M. Gataullin, Y. Ma, A. Mott, H.B. Newman, C. Rogan, M. Spiropulu, V. Timciuc, J. Veverka, R. Wilkinson, S. Xie, Y. Yang, R.Y. Zhu

Carnegie Mellon University, Pittsburgh, USA
B. Akgun, V. Azzolini, A. Calamba, R. Carroll, T. Ferguson, Y. Iiyama, D.W. Jang, Y.F. Liu, M. Paulini, H. Vogel, I. Vorobiev

University of Colorado at Boulder, Boulder, USA
J.P. Cumalat, B.R. Drell, C.J. Edelmaier, W.T. Ford, A. Gaz, B. Heyburn, E. Luiggi Lopez, J.G. Smith, K. Stenson, K.A. Ulmer, S.R. Wagner

Cornell University, Ithaca, USA
J. Alexander, A. Chatterjee, N. Eggert, L.K. Gibbons, B. Heltsley, A. Khukhunaishvili, B. Kreis, N. Mirman, G. Nicolas Kaufman, J.R. Patterson, A. Ryd, E. Salvati, W. Sun, W.D. Teo, J. Thom, J. Thompson, J. Tucker, J. Vaughan, Y. Weng, L. Winstrom, P. Wittich

Fairfield University, Fairfield, USA
D. Winn

Fermi National Accelerator Laboratory, Batavia, USA
S. Abdullin, M. Albrow, J. Anderson, L.A.T. Bauerdick, A. Beretvas, J. Berryhill, P.C. Bhat, I. Bloch, K. Burkett, J.N. Butler, V. Chetluru, H.W.K. Cheung, F. Chlebana, V.D. Elvira, I. Fisk, J. Freeman, Y. Gao, D. Green, O. Gutsche, J. Hanlon, R.M. Harris, J. Hirschauer, B. Hooberman, S. Jindariani, M. Johnson, U. Joshi, B. Kilminster, B. Klima, S. Kunori, S. Kwan, C. Leonidopoulos, J. Linacre, D. Lincoln, R. Lipton, J. Lykken, K. Maeshima, J.M. Marraffino, S. Maruyama, D. Mason, P. McBride, K. Mishra, S. Mrenna, Y. Musienko[52], C. Newman-Holmes, V. O'Dell, O. Prokofyev, E. Sexton-Kennedy, S. Sharma, W.J. Spalding, L. Spiegel, P. Tan, L. Taylor, S. Tkaczyk, N.V. Tran, L. Uplegger, E.W. Vaandering, R. Vidal, J. Whitmore, W. Wu, F. Yang, F. Yumiceva, J.C. Yun

University of Florida, Gainesville, USA
D. Acosta, P. Avery, D. Bourilkov, M. Chen, T. Cheng, S. Das, M. De Gruttola, G.P. Di Giovanni, D. Dobur, A. Drozdetskiy, R.D. Field, M. Fisher, Y. Fu, I.K. Furic, J. Gartner, J. Hugon, B. Kim, J. Konigsberg, A. Korytov, A. Kropivnitskaya, T. Kypreos, J.F. Low, K. Matchev, P. Milenovic[53], G. Mitselmakher, L. Muniz, M. Park, R. Remington, A. Rinkevicius, P. Sellers, N. Skhirtladze, M. Snowball, J. Yelton, M. Zakaria

Florida International University, Miami, USA
V. Gaultney, S. Hewamanage, L.M. Lebolo, S. Linn, P. Markowitz, G. Martinez, J.L. Rodriguez

Florida State University, Tallahassee, USA
T. Adams, A. Askew, J. Bochenek, J. Chen, B. Diamond, S.V. Gleyzer, J. Haas, S. Hagopian, V. Hagopian, M. Jenkins, K.F. Johnson, H. Prosper, V. Veeraraghavan, M. Weinberg

Florida Institute of Technology, Melbourne, USA
M.M. Baarmand, B. Dorney, M. Hohlmann, H. Kalakhety, I. Vodopiyanov

University of Illinois at Chicago (UIC), Chicago, USA
M.R. Adams, I.M. Anghel, L. Apanasevich, Y. Bai, V.E. Bazterra, R.R. Betts, I. Bucinskaite, J. Callner, R. Cavanaugh, O. Evdokimov, L. Gauthier, C.E. Gerber, D.J. Hofman, S. Khalatyan, F. Lacroix, M. Malek, C. O'Brien, C. Silkworth, D. Strom, P. Turner, N. Varelas

The University of Iowa, Iowa City, USA
U. Akgun, E.A. Albayrak, B. Bilki[54], W. Clarida, F. Duru, S. Griffiths, J.-P. Merlo, H. Mermerkaya[55], A. Mestvirishvili, A. Moeller, J. Nachtman, C.R. Newsom, E. Norbeck, Y. Onel, F. Ozok, S. Sen, E. Tiras, J. Wetzel, T. Yetkin, K. Yi

Johns Hopkins University, Baltimore, USA
B.A. Barnett, B. Blumenfeld, S. Bolognesi, D. Fehling, G. Giurgiu, A.V. Gritsan, Z.J. Guo, G. Hu, P. Maksimovic, S. Rappoccio, M. Swartz, A. Whitbeck

The University of Kansas, Lawrence, USA
P. Baringer, A. Bean, G. Benelli, R.P. Kenny Iii, M. Murray, D. Noonan, S. Sanders, R. Stringer, G. Tinti, J.S. Wood, V. Zhukova

Kansas State University, Manhattan, USA
A.F. Barfuss, T. Bolton, I. Chakaberia, A. Ivanov, S. Khalil, M. Makouski, Y. Maravin, S. Shrestha, I. Svintradze

Lawrence Livermore National Laboratory, Livermore, USA
J. Gronberg, D. Lange, D. Wright

University of Maryland, College Park, USA
A. Baden, M. Boutemeur, B. Calvert, S.C. Eno, J.A. Gomez, N.J. Hadley, R.G. Kellogg, M. Kirn,

T. Kolberg, Y. Lu, M. Marionneau, A.C. Mignerey, K. Pedro, A. Peterman, A. Skuja, J. Temple, M.B. Tonjes, S.C. Tonwar, E. Twedt

Massachusetts Institute of Technology, Cambridge, USA
A. Apyan, G. Bauer, J. Bendavid, W. Busza, E. Butz, I.A. Cali, M. Chan, V. Dutta, G. Gomez Ceballos, M. Goncharov, K.A. Hahn, Y. Kim, M. Klute, K. Krajczar[56], W. Li, P.D. Luckey, T. Ma, S. Nahn, C. Paus, D. Ralph, C. Roland, G. Roland, M. Rudolph, G.S.F. Stephans, F. Stöckli, K. Sumorok, K. Sung, D. Velicanu, E.A. Wenger, R. Wolf, B. Wyslouch, M. Yang, Y. Yilmaz, A.S. Yoon, M. Zanetti

University of Minnesota, Minneapolis, USA
S.I. Cooper, B. Dahmes, A. De Benedetti, G. Franzoni, A. Gude, S.C. Kao, K. Klapoetke, Y. Kubota, J. Mans, N. Pastika, R. Rusack, M. Sasseville, A. Singovsky, N. Tambe, J. Turkewitz

University of Mississippi, University, USA
L.M. Cremaldi, R. Kroeger, L. Perera, R. Rahmat, D.A. Sanders

University of Nebraska-Lincoln, Lincoln, USA
E. Avdeeva, K. Bloom, S. Bose, J. Butt, D.R. Claes, A. Dominguez, M. Eads, J. Keller, I. Kravchenko, J. Lazo-Flores, H. Malbouisson, S. Malik, G.R. Snow

State University of New York at Buffalo, Buffalo, USA
U. Baur, A. Godshalk, I. Iashvili, S. Jain, A. Kharchilava, A. Kumar, S.P. Shipkowski, K. Smith

Northeastern University, Boston, USA
G. Alverson, E. Barberis, D. Baumgartel, M. Chasco, J. Haley, D. Nash, D. Trocino, D. Wood, J. Zhang

Northwestern University, Evanston, USA
A. Anastassov, A. Kubik, N. Mucia, N. Odell, R.A. Ofierzynski, B. Pollack, A. Pozdnyakov, M. Schmitt, S. Stoynev, M. Velasco, S. Won

University of Notre Dame, Notre Dame, USA
L. Antonelli, D. Berry, A. Brinkerhoff, M. Hildreth, C. Jessop, D.J. Karmgard, J. Kolb, K. Lannon, W. Luo, S. Lynch, N. Marinelli, D.M. Morse, T. Pearson, M. Planer, R. Ruchti, J. Slaunwhite, N. Valls, M. Wayne, M. Wolf

The Ohio State University, Columbus, USA
B. Bylsma, L.S. Durkin, C. Hill, R. Hughes, K. Kotov, T.Y. Ling, D. Puigh, M. Rodenburg, C. Vuosalo, G. Williams, B.L. Winer

Princeton University, Princeton, USA
N. Adam, E. Berry, P. Elmer, D. Gerbaudo, V. Halyo, P. Hebda, J. Hegeman, A. Hunt, P. Jindal, D. Lopes Pegna, P. Lujan, D. Marlow, T. Medvedeva, M. Mooney, J. Olsen, P. Piroué, X. Quan, A. Raval, B. Safdi, H. Saka, D. Stickland, C. Tully, J.S. Werner, A. Zuranski

University of Puerto Rico, Mayaguez, USA
J.G. Acosta, E. Brownson, X.T. Huang, A. Lopez, H. Mendez, S. Oliveros, J.E. Ramirez Vargas, A. Zatserklyaniy

Purdue University, West Lafayette, USA
E. Alagoz, V.E. Barnes, D. Benedetti, G. Bolla, D. Bortoletto, M. De Mattia, A. Everett, Z. Hu, M. Jones, O. Koybasi, M. Kress, A.T. Laasanen, N. Leonardo, V. Maroussov, P. Merkel, D.H. Miller, N. Neumeister, I. Shipsey, D. Silvers, A. Svyatkovskiy, M. Vidal Marono, H.D. Yoo, J. Zablocki, Y. Zheng

Purdue University Calumet, Hammond, USA
S. Guragain, N. Parashar

Rice University, Houston, USA
A. Adair, C. Boulahouache, K.M. Ecklund, F.J.M. Geurts, B.P. Padley, R. Redjimi, J. Roberts, J. Zabel

University of Rochester, Rochester, USA
B. Betchart, A. Bodek, Y.S. Chung, R. Covarelli, P. de Barbaro, R. Demina, Y. Eshaq, T. Ferbel, A. Garcia-Bellido, P. Goldenzweig, J. Han, A. Harel, D.C. Miner, D. Vishnevskiy, M. Zielinski

The Rockefeller University, New York, USA
A. Bhatti, R. Ciesielski, L. Demortier, K. Goulianos, G. Lungu, S. Malik, C. Mesropian

Rutgers, the State University of New Jersey, Piscataway, USA
S. Arora, A. Barker, J.P. Chou, C. Contreras-Campana, E. Contreras-Campana, D. Duggan, D. Ferencek, Y. Gershtein, R. Gray, E. Halkiadakis, D. Hidas, A. Lath, S. Panwalkar, M. Park, R. Patel, V. Rekovic, J. Robles, K. Rose, S. Salur, S. Schnetzer, C. Seitz, S. Somalwar, R. Stone, S. Thomas

University of Tennessee, Knoxville, USA
G. Cerizza, M. Hollingsworth, S. Spanier, Z.C. Yang, A. York

Texas A&M University, College Station, USA
R. Eusebi, W. Flanagan, J. Gilmore, T. Kamon[57], V. Khotilovich, R. Montalvo, I. Osipenkov, Y. Pakhotin, A. Perloff, J. Roe, A. Safonov, T. Sakuma, S. Sengupta, I. Suarez, A. Tatarinov, D. Toback

Texas Tech University, Lubbock, USA
N. Akchurin, J. Damgov, C. Dragoiu, P.R. Dudero, C. Jeong, K. Kovitanggoon, S.W. Lee, T. Libeiro, Y. Roh, I. Volobouev

Vanderbilt University, Nashville, USA
E. Appelt, A.G. Delannoy, C. Florez, S. Greene, A. Gurrola, W. Johns, C. Johnston, P. Kurt, C. Maguire, A. Melo, M. Sharma, P. Sheldon, B. Snook, S. Tuo, J. Velkovska

University of Virginia, Charlottesville, USA
M.W. Arenton, M. Balazs, S. Boutle, B. Cox, B. Francis, J. Goodell, R. Hirosky, A. Ledovskoy, C. Lin, C. Neu, J. Wood, R. Yohay

Wayne State University, Detroit, USA
S. Gollapinni, R. Harr, P.E. Karchin, C. Kottachchi Kankanamge Don, P. Lamichhane, A. Sakharov

University of Wisconsin, Madison, USA
M. Anderson, D. Belknap, L. Borrello, D. Carlsmith, M. Cepeda, S. Dasu, E. Friis, L. Gray, K.S. Grogg, M. Grothe, R. Hall-Wilton, M. Herndon, A. Hervé, P. Klabbers, J. Klukas, A. Lanaro, C. Lazaridis, J. Leonard, R. Loveless, A. Mohapatra, I. Ojalvo, F. Palmonari, G.A. Pierro, I. Ross, A. Savin, W.H. Smith, J. Swanson

†: Deceased
1: Also at Vienna University of Technology, Vienna, Austria
2: Also at National Institute of Chemical Physics and Biophysics, Tallinn, Estonia
3: Also at Universidade Federal do ABC, Santo Andre, Brazil
4: Also at California Institute of Technology, Pasadena, USA

5: Also at CERN, European Organization for Nuclear Research, Geneva, Switzerland
6: Also at Laboratoire Leprince-Ringuet, Ecole Polytechnique, IN2P3-CNRS, Palaiseau, France
7: Also at Suez Canal University, Suez, Egypt
8: Also at Zewail City of Science and Technology, Zewail, Egypt
9: Also at Cairo University, Cairo, Egypt
10: Also at Fayoum University, El-Fayoum, Egypt
11: Also at British University, Cairo, Egypt
12: Now at Ain Shams University, Cairo, Egypt
13: Also at National Centre for Nuclear Research, Swierk, Poland
14: Also at Université de Haute-Alsace, Mulhouse, France
15: Now at Joint Institute for Nuclear Research, Dubna, Russia
16: Also at Moscow State University, Moscow, Russia
17: Also at Brandenburg University of Technology, Cottbus, Germany
18: Also at Institute of Nuclear Research ATOMKI, Debrecen, Hungary
19: Also at Eötvös Loránd University, Budapest, Hungary
20: Also at Tata Institute of Fundamental Research - HECR, Mumbai, India
21: Also at University of Visva-Bharati, Santiniketan, India
22: Also at Sharif University of Technology, Tehran, Iran
23: Also at Isfahan University of Technology, Isfahan, Iran
24: Also at Plasma Physics Research Center, Science and Research Branch, Islamic Azad University, Teheran, Iran
25: Also at Facoltà Ingegneria Università di Roma, Roma, Italy
26: Also at Università della Basilicata, Potenza, Italy
27: Also at Università degli Studi Guglielmo Marconi, Roma, Italy
28: Also at Università degli studi di Siena, Siena, Italy
29: Also at University of Bucharest, Faculty of Physics, Bucuresti-Magurele, Romania
30: Also at Faculty of Physics of University of Belgrade, Belgrade, Serbia
31: Also at University of California, Los Angeles, Los Angeles, USA
32: Also at Scuola Normale e Sezione dell' INFN, Pisa, Italy
33: Also at INFN Sezione di Roma; Università di Roma "La Sapienza", Roma, Italy
34: Also at University of Athens, Athens, Greece
35: Also at Rutherford Appleton Laboratory, Didcot, United Kingdom
36: Also at The University of Kansas, Lawrence, USA
37: Also at Paul Scherrer Institut, Villigen, Switzerland
38: Also at Institute for Theoretical and Experimental Physics, Moscow, Russia
39: Also at Gaziosmanpasa University, Tokat, Turkey
40: Also at Adiyaman University, Adiyaman, Turkey
41: Also at Izmir Institute of Technology, Izmir, Turkey
42: Also at The University of Iowa, Iowa City, USA
43: Also at Mersin University, Mersin, Turkey
44: Also at Ozyegin University, Istanbul, Turkey
45: Also at Kafkas University, Kars, Turkey
46: Also at Suleyman Demirel University, Isparta, Turkey
47: Also at Ege University, Izmir, Turkey
48: Also at School of Physics and Astronomy, University of Southampton, Southampton, United Kingdom
49: Also at INFN Sezione di Perugia; Università di Perugia, Perugia, Italy
50: Also at University of Sydney, Sydney, Australia
51: Also at Utah Valley University, Orem, USA

52: Also at Institute for Nuclear Research, Moscow, Russia
53: Also at University of Belgrade, Faculty of Physics and Vinca Institute of Nuclear Sciences, Belgrade, Serbia
54: Also at Argonne National Laboratory, Argonne, USA
55: Also at Erzincan University, Erzincan, Turkey
56: Also at KFKI Research Institute for Particle and Nuclear Physics, Budapest, Hungary
57: Also at Kyungpook National University, Daegu, Korea